ABSTRACT

HOLMES, THOMAS WESLEY. Shielded Source Analysis using Precalculated Library Estimates. (Under the direction of Robin Gardner.)

In this work, an approach was developed for automatically determining the source intensity of an unknown shielded source by first determining the thicknesses of three different shielding materials from a passively collected gamma-ray spectrum by making comparisons with predetermined shielded spectra. These evaluations were dependent on the accuracy and validity of the predetermined library spectra which were created by changing the thicknesses of lead, aluminum and wood that was used to simulate any actual shielding. The materials were held in the same respective order from source to detector where each material consisted of three individual thicknesses. This then produced two separate data sets of 27 total shielding material situations and subsequent predetermined libraries that were created for each radionuclide source used. The technique used to calculate the thicknesses of the materials employs first a traditional linear stripping technique with a different set of unshielded radioisotopes. This then uses the full width at half of the maximum (FWHM) value for each found peak value and compares it to a predetermined equation to ensure that the peak was not convolved with another one. After determining that the found peak was not convolved, a Levenberg-Marquardt nonlinear search that employed tri-linear interpolation with the respective predetermined libraries within each channel for the supplied input spectrum. This produces several possibilities for answers; therefore, a series of tests were created to ensure the correctness of the solution to the problem. Under situations with sufficient information known about the detection situation at hand, the method was shown to behave in a manner that produces reasonable results and can serve as a good preliminary solution.

Shielded Source Analysis using Precalculated Library Estimates

by
Thomas Wesley Holmes

A thesis submitted to the Graduate Faculty of
North Carolina State University
in partial fulfillment of the
requirements for the Degree of
Master of Science

Nuclear Engineering

Raleigh, North Carolina

2013

APPROVED BY:

John Mattingly	David Lalush
Dean Mitchell	Robin Gardner Chair of Advisory Committee

BIOGRAPHY

Thomas Wesley Holmes was born in Raleigh, NC on the 31^{st} of October, 1986. He received his Bachelors of Science in nuclear engineering with a minor in graphic communications in the fall of 2009. During this work, he decided to pursue higher education.

ACKNOWLEDGEMENTS

I would like to thank my advisor for his help, my family for their unwavering love and support and my friends for some much needed relief. Also, Sara, my favorite, thank you.

TABLE OF CONTENTS

LIST OF TABLES

LIST OF FIGURES

Chapter 1

Introduction

In many common real world situations, analysis of gamma spectra is needed in circumstances that contain unknown shielding materials with an associated unknown thickness that includes an unknown source and strength. This problem becomes more complicated when there are perturbations in the known background that stem from an array of unforeseeable circumstances. The long list of unknown parameters causes the pathway for any solution to require a variety of techniques for determining these factors.

In this discussion, the main focus will be placed on the situation of a shipping cargo container but the overall approach can be applied to a variety of problems. Cargo containers are of special importance because a common fear when dealing with incoming cargo containers, both domestic and international, is the threat of clandestine nuclear materials. With this possibility in mind, it would only make logical sense to use the most accurate tools available for more precisely assessing the potential presence of malicious nuclear materials within any container.

The problem of analyzing cargo containers can often be modeled in a combination of linear and non-linear parameters in terms of the radionuclides present, their source

intensity and the shielding materials at hand. Several approaches for determining the various radionuclides within any given spectrum have implemented the method of least squares analysis. Salmon was a primary contributor to this approach in 1961 where he established its ability to successfully determine the composition and contribution of a spectrum with six separate sources and their associated spectra. He was able to complete this task by recognizing that the Compton continuum of the higher energy photo peaks impacted the shape of the lower energy peaks. To account for this, he used the entire spectrum of all of the radioisotopes found within the spectrum in his calculations. This successful demonstration of the least squares approach has lead to similar techniques that have been applied previously at NC State University for the measurement applications of prompt gamma-ray neutron activation analysis and x-ray fluorescence spectroscopy for elemental analysis (Guo, Gardner).

In order to first determine which radioisotopes are present in a given spectrum, the simplest approach is to identify each full energy peak. Based on these full energy peaks and their relative intensity, corresponding radioisotope signature patterns can be found. The basic count rates over these full energy peaks can be attributed to the relative activity concentration after background has been subtracted from the spectrum. This type of spectral deconvolution is performed using knowledge of the signature spectral response of the types of sources that should and could be present within the given situation. Spectral stripping is known as the peeling away each radionuclide spectral component from the original spectrum over the entire energy space starting from the highest energy and moving downward. As noted by Allyson, the use of the stripping technique is limited in its ability to represent artificial scattering of the source particles interacting with materials before being collected.

There is a fundamental issue when attempting to resolve these various unknown

shielding materials and their associated unknown thicknesses when given a spectrum of an unknown source and activity, which is centered on the idea that the peak value does not contain all of this information. The principal means by which to identify a source is by its high intensity photo-peaks but in the situation that there is little to no knowledge of several shielding materials and the initial source strength, a complex density transmission gage using these photo-peaks is not possible after source identification. The most appropriate means to determine the shielding material is to consider the portion of the spectrum that has interacted with the material, scattered and then been collected by the detector. Due to the range of incident energies considered in this application the region that needs to be considered for shielding material identification is from incoherent scattering events which are dominated by Compton scattering that reside below the full energy photo-peak.

In the past, a solution to determining the presence of nuclear materials within cargo containers considered that the shape of the various components used to shield or hide the nuclear materials from detection was negligible when constructing the database of simulation results (Gardner, 1991). This is known as a one dimensional (1D) approach. An updated approach builds on this previous idea but in this modified instance, the shape of the various components within the cargo container used to shield the source was taken into consideration. This case is known as a three dimensional (3D) approach. A primary reason that this advance was deemed as an essential component in the detection of nuclear materials was due to the expected increase in the accuracy of the measurements. To demonstrate the difference in these two approaches, two MCNP5 v. 1.51 simulations were performed where the shape of two otherwise identical systems, one constructed in a 1D fashion and the other in a 3D fashion, were simulated. The shielding materials used were lead, aluminum and wood, in the order that the radiation passed from source

to detector, where each case contained the same thickness of each but the shape of the shielding materials varied between the two scenarios. The 1D case consisted of three concentric spheres and the 3D case consisted of the first two shielding materials (lead and aluminum) as right circular cylindrical cans and the outer most shield of wood in the shape of a square box. The geometric description of each can be found in figures 1 and their corresponding detector outputs are given in figure 2. The source used in these simulations was ^{137}Cs which was placed in the center of the system and a 2 X 4 X 16 box style NaI(Tl) detector was placed 75 cm from the source with the 4 X 16 side facing the system.

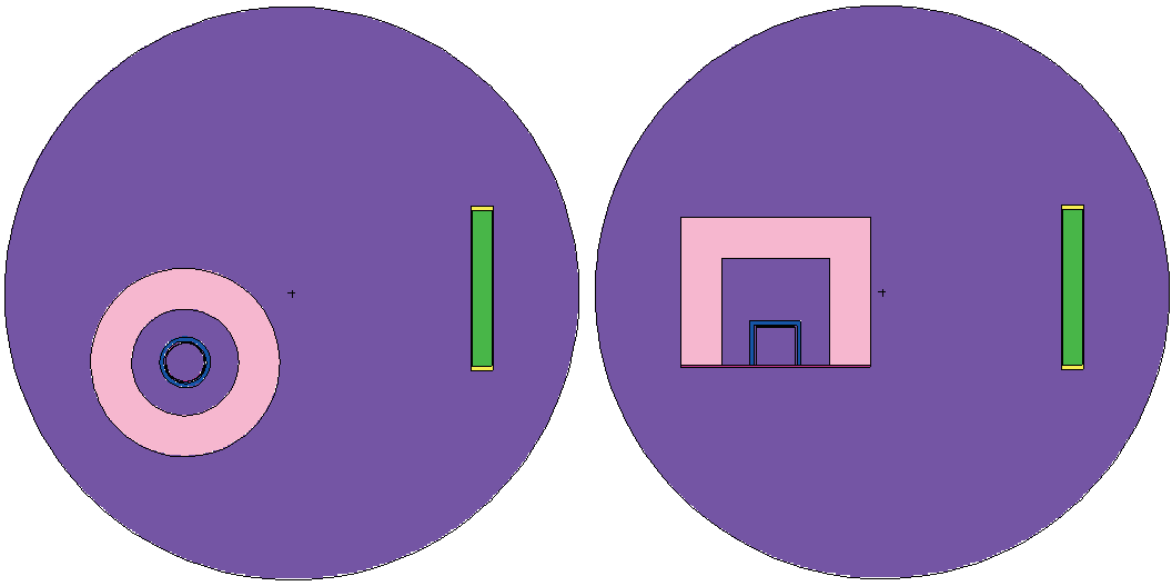

Figure 1.1: Side views of the 1D configuration and the 3D configuration respectively.

Within the simulated detector responses (Gardner, 2004), there was a noticeable difference along the Compton continuum which was directly related to the geometric

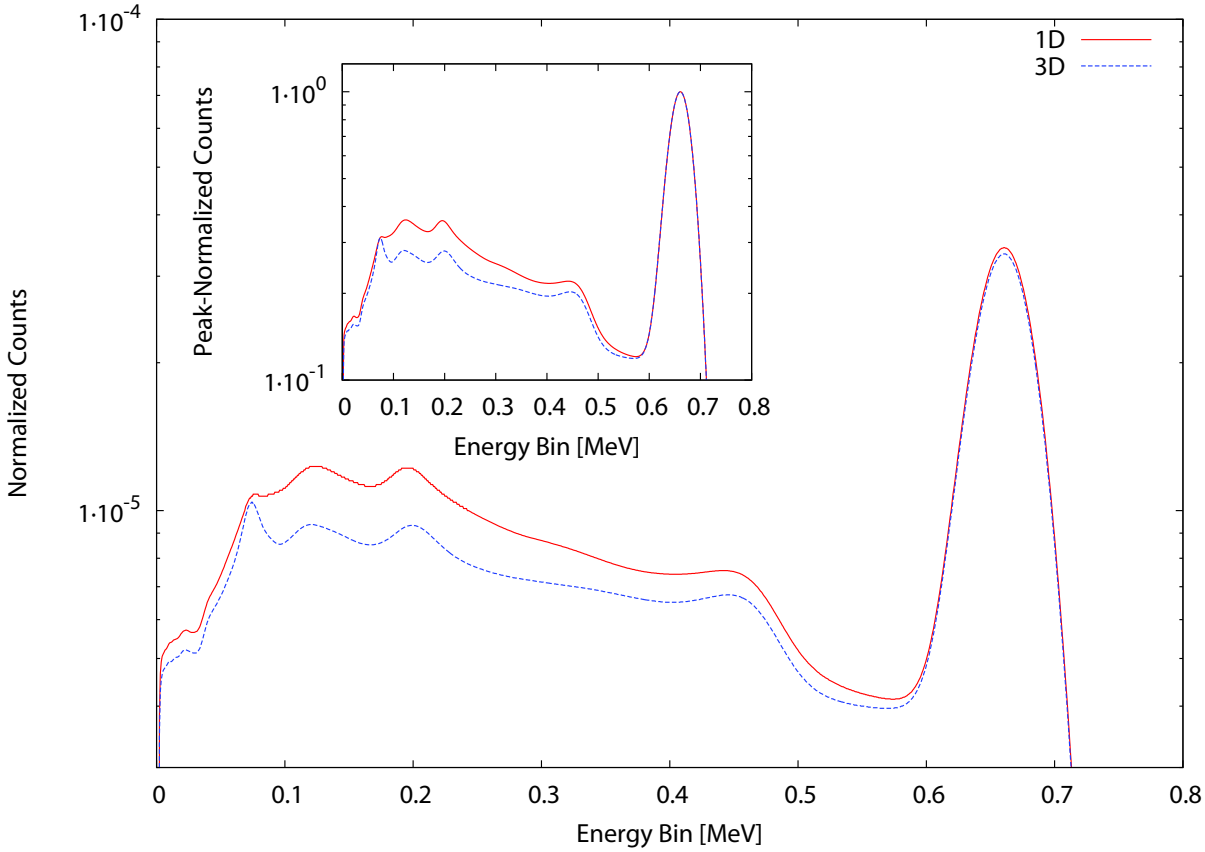

Figure 1.2: Comparison of the detector outputs from the 1D and 3D simulations.

conditions being altered. These preliminary results then deemed it appropriate to produce a new and improved library of conditions for the inverse analysis.

Chapter 2

MCLLS and Library Setup

The primary tool used in this evaluation of the differences in shielding materials employs the Monte Carlo Library Least Squares (MCLLS) method. This approach uses a series of libraries based on very accurate pre-calculated forward models to fit an unknown data set which in this case is a spectrum (Gardner, Sood, 97). This method is very useful in evaluating inverse spectral problems and while it may require more effort than peak transmission gauges, it is more advantageous in that it uses the entire spectral data available and generates better accuracy of its solution (Metwally). This technique has proven itself to be successful for the inverse elemental analysis of prompt gamma-ray neutron activation analysis and energy-dispersive X-ray fluorescence analyzers (Gardner, Sood, 04).

As a means to use the MCLLS process, a generalized FORTRAN code has been developed by Gardner for determining the parameters of a fitting model for a given data set. This package has been called CURMOD, which is based on the CURFIT subroutine developed by Bevington, and has served as the backbone for many specialized code developments. CURMOD can be used to describe a data set using any combination of linear

and non-linear parameters. Accurate guesses are required for each non-linear parameter but they are not required for the linear parameters. CURMOD uses the Levenberg-Marquardt non-linear search method for finding a solution to the non-linear parameters and a multiple linear regression in determination of the linear parameters. It uses a minimized reduced χ^2 found in the following equation to select the best fit for all of the parameter values.

$$\chi^2_{red} = \frac{\chi^2}{\nu} = \frac{1}{\nu}\sum \frac{(O-E)^2}{\sigma^2} \tag{2.1}$$

Where ν is the number of degrees of freedom, σ^2 is the variance of the observation, O is the observed data and E is the theoretical data. Also CURMOD quantifies the error associated with each parameter for the final fit to the input data set.

Given the problem at hand, where there is a combination of unknown shielding materials along with an unknown radionuclide and source strength, the linear and non-linear parameters must be reduced to produce a generalized situation that can be resolved. These simplifications were based around the operating conditions for the primary devices currently used for cargo monitoring that are probably akin to the nightmares of those that dream of precise and stable laboratory measurements. The contents of the sample (or cargo container) are usually of largely unknown composition and geometry. If illicit radioactive materials are intentionally present, they are likely to be concealed using unknown shielding materials and in many cases it is not feasible to perfectly control the speed and positioning of the container passing through the monitor.

The essential forward simulation problem is used to accurately determine the photon flux and energy distribution entering the detector surface. The key ideas to this problem

are variable amounts of unknown shielding, with a distance on the order of meters between the source and detector. The scheme depicted in the following figure is a cross sectional view of what was developed with these characteristics in mind.

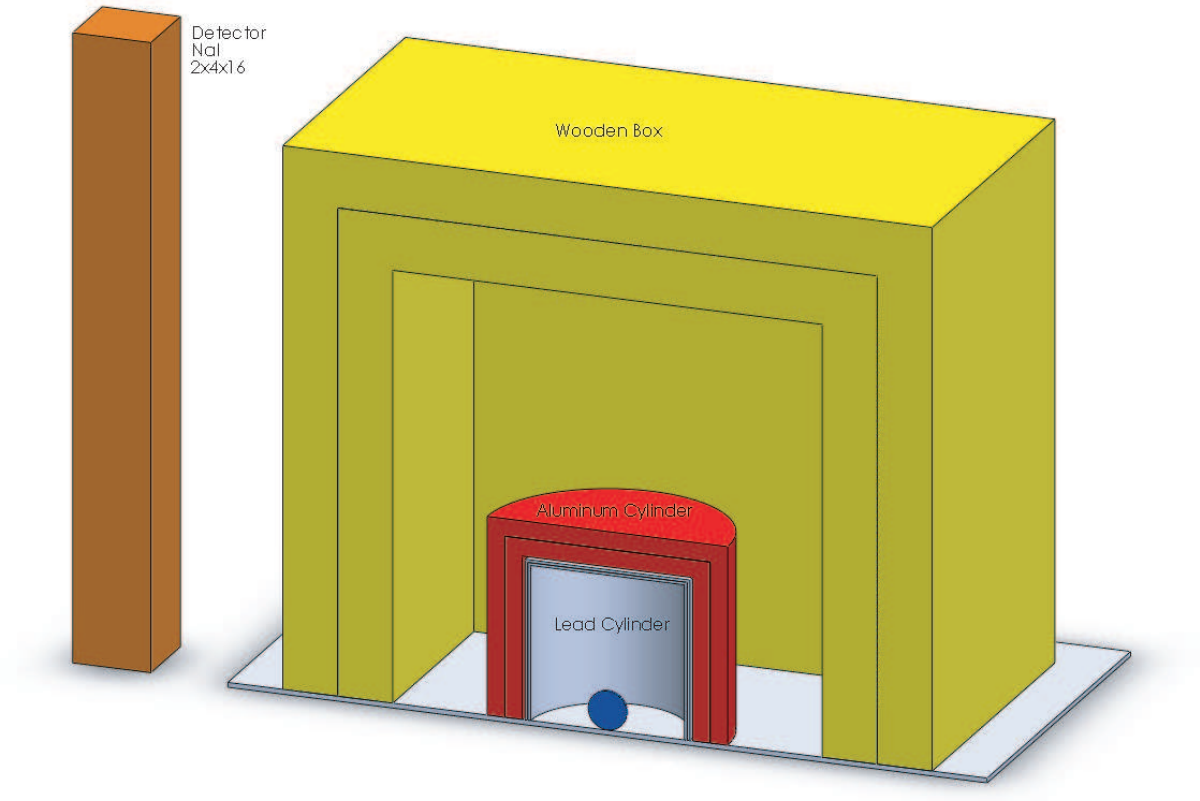

Figure 2.1: A crossectional view (diagram) of the benchmark configuration with all materials in the standard position.

This design included three different shielding materials of lead, aluminum and wood with each having three equally thick shielding components and a null condition where the material is entirely removed. The inner two materials were in the shape of a right cylindrical cans and the outer most shielding material was in the shape of a cube. The

detector used was a 2 X 4 X 16 box style NaI(Tl) detector that was placed one meter from the point source located in the center of the system.

The idea of using multiple shielding materials to determine the composition of any absorbing material was first conceptualized by Estep and Sapp. This approach was called the material basis set method and was based on the effective atomic number principle. This principle considered that the attenuation properties of gamma rays though any element could be closely approximated by a combination of basis materials mixed in the appropriate proportions. It was proposed that in most applications, two materials were sufficient in producing an equivalent attenuation map but this idea was expanded upon in this specific application by adding a third member to the basis materials and adding multiple thicknesses of these materials. This improvement was selected to gain added accuracy to the final result, allow for a larger range of possibilities and span a wider atomic number range of shielding materials. The overall effective material thicknesses will also produce an equivalent scaling factor that can be used to determine the strength of the source being detected.

Variable shielding thickness was evoked by allowing each of the three shielding materials to possess three layers of equal thickness. For example, each of the lead layers has a thickness of 0.179 cm and the combination of three of these thicknesses results in a total thickness of 0.537 cm. For each material, the combination of the middle layer and inner layer was considered the standard thickness. The middle layer alone was denoted as -50% of the standard thickness. The combination of all three layers was denoted as +50% of the standard thickness. In all of the simulations considered, there were between one and three layers of each of the three shielding materials present. The fully factorial design then resulted in a data set of 27 unique combinations using all three thicknesses of the three shielding materials. When the null condition was included, this created a separate

data set of 27 unique combinations where the thicknesses of the materials range from no thickness to the standard thickness.

The total thickness of each separate shielding material was calculated so that half of the incident number of gamma rays would be lost upon leaving the material using the general mass attenuation equation.

$$I = I_0 e^{-(\frac{\mu}{\rho})\rho t} \tag{2.2}$$

The values for the mass attenuation coefficient were chosen for each material at the primary decay energy of ^{137}Cs at 661.7 keV. This idea came from the desire to turn this simulation into a physical experiment in the future. The reason this scheme was chosen was to maintain the thickness of the shielding at realistic dimensions and also to not force the activity of the source in the physical experiment into an unsafe intensity range in order to detect a sufficient number of particles in a reasonable measurement time. The lowest counting rate resulted when all the possible shielding material was present which gave a gamma-ray intensity of one eighth the original incident intensity.

In order to relieve confusion among readers and the authors about the various shielding configurations, the following naming convention was preferred. Each configuration was denoted with a three letter descriptor. Each letter in the descriptor denotes the thickness of shielding present for one material. The letter m (for minus) denotes a -50% thickness from standard, or one layer. The letter s (for standard) indicates the standard thickness, or two layers. The letter p (for plus) represents a +50% thickness, or three layers. Using 0 signifies the lack of the shielding material present in the forward calculation. The meanings of the letters in the configuration descriptor apply to the shielding

Table 2.1: Dimensions of the Shielding Materials

	Pb [cm]	Al [cm]	Wood [cm]
+50%			
Top	10.5375	13.9599	38.643
Bottom	10.0000	10.5375	27.919
Outer	5.5375	8.9599	24.684
Inner	5.0000	5.5375	13.959
Standard			
Top	10.3584	12.8191	35.069
Bottom	10.0000	10.5375	27.919
Outer	5.3584	7.8191	21.109
Inner	5.0000	5.5375	13.959
-50%			
Top	10.1792	11.6783	31.494
Bottom	10.0000	10.5375	27.919
Outer	5.1792	6.6783	17.534
Inner	5.0000	5.5375	13.959

materials in the order: lead, aluminum, and then wood as in the pathway of the radiation from the source to the detector. Accordingly, sss stands for the standard thickness for all shielding materials, and msp denotes -50% thickness of lead followed by a standard thickness of aluminum followed by +50% thickness of wood. The exact dimensions and shield thicknesses of the scheme are given in Tables 2.1 and 2.2 respectively.

Each of the two data sets consisting of 27 individual libraries was created for three separate sources: ^{137}Cs, ^{60}Co and ^{238}U. Ultimately, this consisted of a total of 138 non-repeated spectra for the entire data used in this exercise.

Table 2.2: Thicknesses of the Shielding Materials

	Pb [cm]	Al [cm]	Wood [cm]
+50%	0.5375	3.4224	10.7241
Standard	0.3584	2.2816	7.1494
-50%	0.1792	1.1408	3.5747

Chapter 3

Library Creation

All of the libraries were calculated with MCNP5 v1.60 in 'mode p e' on the CEAR high performance computing cluster of 164 computers in its optimal configuration. All of the cells within the input deck were labeled with a photon and electron importance of 1 to help ensure the overall validity of the answers generated. The development of the in house Linux CEAR cluster has been a primary factor in allowing faster calculations for these types of complex problems. The F8 deposited photon energy tally over 512 energy bins, equally and linearly spaced between 0 and 3.0 MeV, was used to estimate energy distribution of pulses crated in the detector over the entire energy range. A pure analog tally was collected for each simulation.

The spectra were spread using a post-processing technique for simulating the detector response function to help take full advantage of the natural smoothing effect of the Gaussian broadening effect (Metwally, 2004). This approach to spreading the spectrum at the end of the simulation rather than history by history, has been found to increase the overall efficiency of the simulation by approximately two orders of magnitude in computation time (Metwally, 2004). These spreading parameters were generated from

experimentally collected data where the full width at half of the maximum value at the full energy photo peaks were computed over a wide range of energies. The detector resolution was generated in terms of the standard deviation of a Gaussian distribution. These standard deviations were created by using the power-law form given in the flowing equation.

$$\sigma = aE^b \tag{3.1}$$

Where σ is the standard deviation in MeV, E is the energy of the gamma-ray in MeV and a and b are the empirical constants found from experimental data. The detector response function model was then used to broaden the spectrum with the Gaussian distribution that used the form from the previous equation. The empirical values used in these calculations were found from using the full energy photo peaks and their associated FWHM of the following sources: ^{137}Cs, ^{60}Co, ^{46}Sc, ^{22}Na, ^{133}Ba. The calculated FWHM values for each of the found peaks are shown in table 3.1.

In order to calculate the empirical values, a linear trend was created after taking the natural log of the centroids and their associated FWHM. These calculated values can be found in figure 3.1 plotted along with its linear trend fit using the subsequent equation. The slope, m, had a value of 0.654 and a y-intercept, b, of -3.3149 with an associated R^2 value of 0.984.

$$y = mx + b \tag{3.2}$$

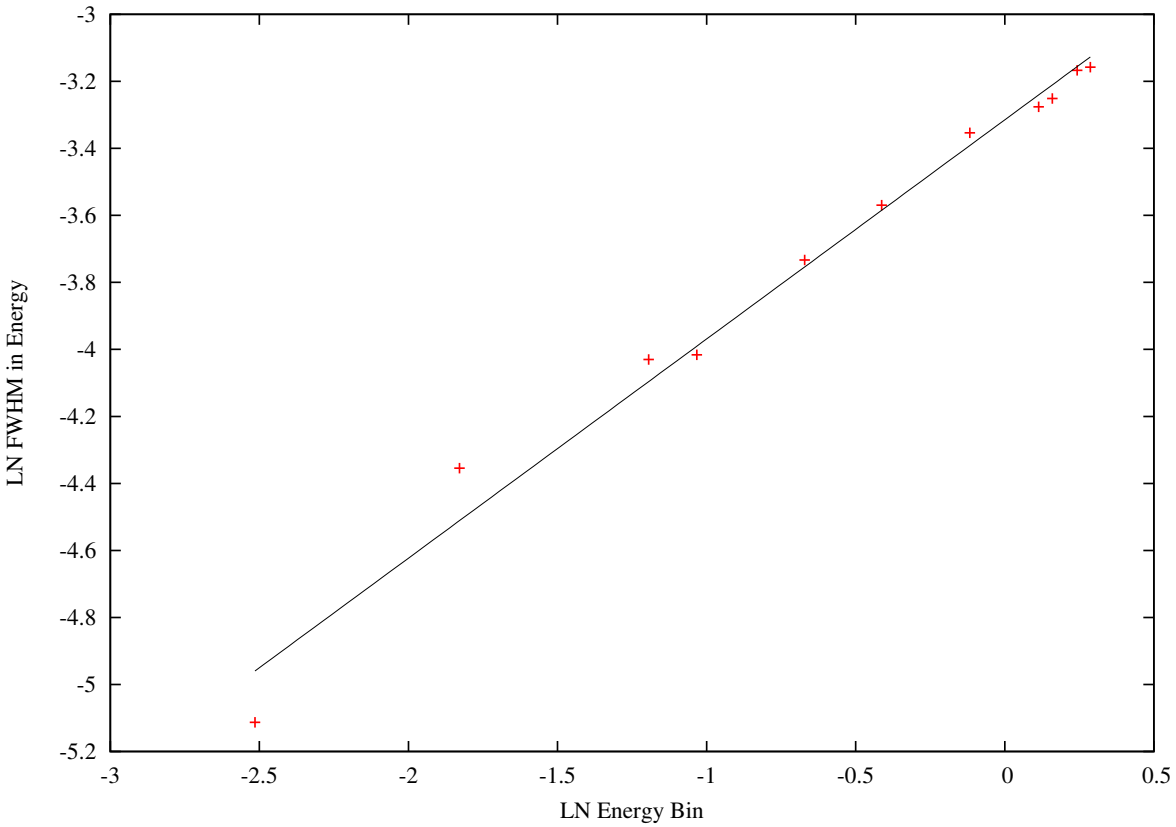

Figure 3.1: Natural Log of Centroids V.S. FWHM and its Linear Trend

Table 3.1: Sources with their associated centroids and associated FWHM in MeV

	Centroid	FWHM
Co60	1.173	0.039
	1.333	0.043
Cs137	0.662	0.028
Sc46	0.889	0.035
	1.121	0.038
Na22	0.511	0.024
	1.275	0.042
Ba133	0.081	0.006
	0.161	0.013
	0.303	0.018
	0.356	0.018

The parameters used in calculating the standard deviation for the Gaussian spreading of the spectrum were found by substituting the slope of the linear trend for the parameter a in the standard deviation equation. The value b is found by taking the exponential of the y-intercept value. These values are specific for each type of detector based on their geometry, density, crystal structured and elemental composition. In this particular application the equation used in the post processed Gaussian spreading routine for generating the appropriate standard deviation is as in equation 3.3. These parameters were applied to all of the libraries created.

$$\sigma = 0.654E^{0.036337} \tag{3.3}$$

Now that the shielding materials and their multiple layers of varying thickness have

been created along with the post processed detector response parameters, the individual source specifications must be made to simulate the three radioisotopes used in this application. These source specifications included all of the photon emissions from ^{137}Cs and ^{60}Co that were above an intensity of 0.0001. A sample input deck for MCNP of the sss configuration using ^{137}Cs as the source can be found in the appendix. All other input decks will be omitted due to the fact that the variations of the shielding material thickness can easily be changed from this base configuration. Upon completing the simulations for all 27 of the variations of thicknesses of the materials for one data set, it was desired to find correlations of the thickness to the changes in the spectra. In order to find these correlations all of the spectra were plotted on one graph. Several trends were appearing but to further exaggerate the connections, each of the spectra were normalized to its own peak value. Figure 3.2 demonstrates the output from MCNP that have been spread using the post processing technique and figure 3.3 shows the peak normalized spectra to the data set using ^{137}Cs ranging from the mmm to ppp configurations. Each of the simulated spectra used 750000000 histories and produced a relative error less than 2% for each energy bin.

Figure 3.2 shows separate groupings over the Compton continuum where each of the three major groupings shares the same lead configuration as denoted by the line type This was especially true over the range of approximately 0.2 to 0.4 MeV. Figure 3.3 also shows separate groupings over the Compton continuum where each group shares the same configuration of aluminum and wood through usage of the same color. The only difference within the nine groups depends on the thickness of the lead which is distinguished by the line type. The second data set of 27 spectra using ^{137}Cs was created over the configurations of the null conditions to the sss configuration. As with the previous data set, each of the simulated spectra used 750000000 histories and produced a relative

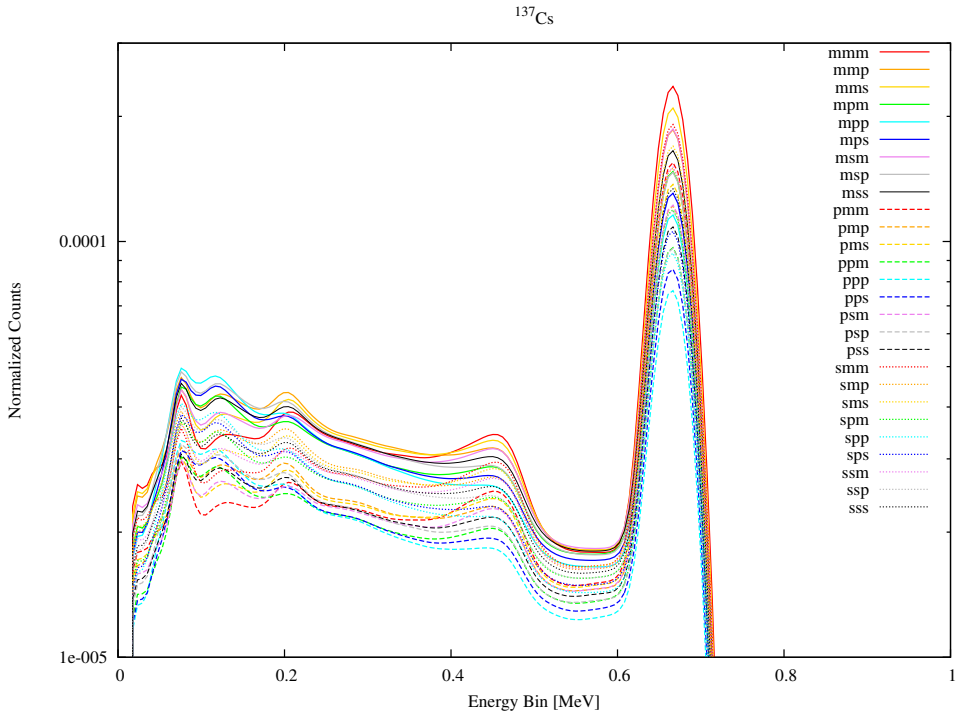

Figure 3.2: Data Set from 'mmm' to 'ppp' Configurations using ^{137}Cs

error less than 2% for each energy bin. All subsequent figures depicting various library data sets will maintain the same color schemes and line types in the same order of relative material thickness to the data set as with the previous figures. As with the previous data set, figure 3.4 shows that there are three groupings based off of the thickness of the lead used found along the range from approximately 0.2 to 0.4 MeV. Given the situation that there is no lead shielding present, the low energy photons produced from the source are sufficiently collected but when the higher density shielding materials are added, the collected photons readily decrease. It should also be noted that within these data sets, the unshielded spectrum is included as the 000 case. Figure 3.5 more clearly demonstrates that the lack of shielding material present reduces the individualistic properties of the spectra generated. This has to do with the lack of overall interactions that the photons experience before collection.

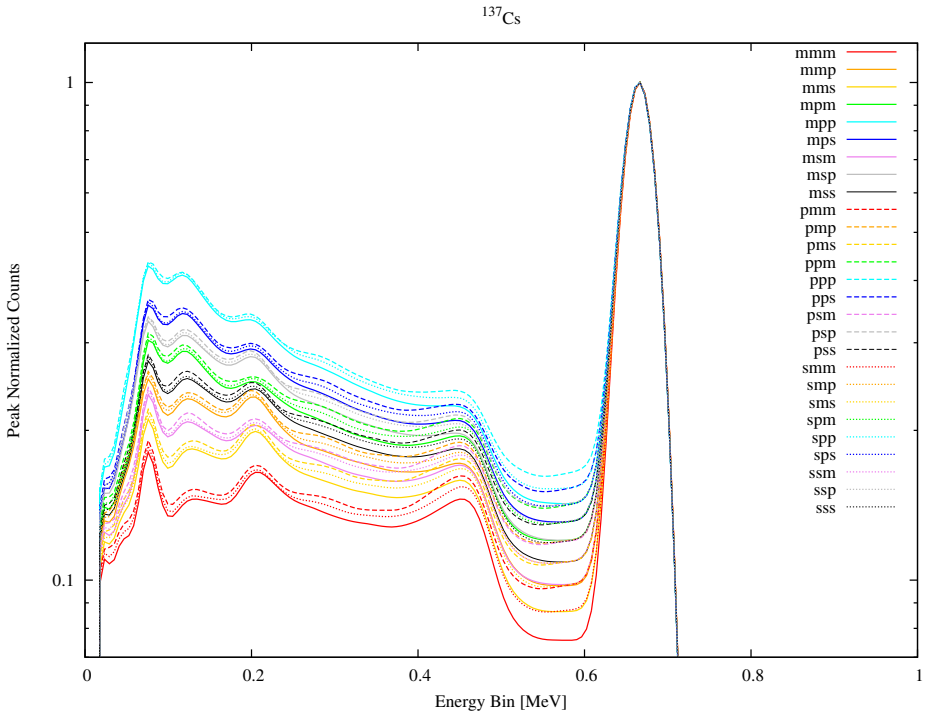

Figure 3.3: Peak Normalized Data Set from mmm to ppp Configurations using ^{137}Cs

Next, the data set using ^{60}Co ranging from the mmm to ppp configurations are shown. The source energy intensity and probability distribution were defined within MCNP as follows:

```
si1  L 1.173237 1.332501
sp1  D 0.999736 0.9998561
```

Figure 3.7 demonstrates that again there are similarities between the relationships based on the nine different combinations of aluminum and wood and within those groups there are distinctions on the thickness of lead used.

Again, the second data set of 27 spectra using ^{60}Co was created over the configurations of the null conditions to the sss configuration. As with the previous data set, each of the simulated spectra used 750000000 histories and produced a relative error less than

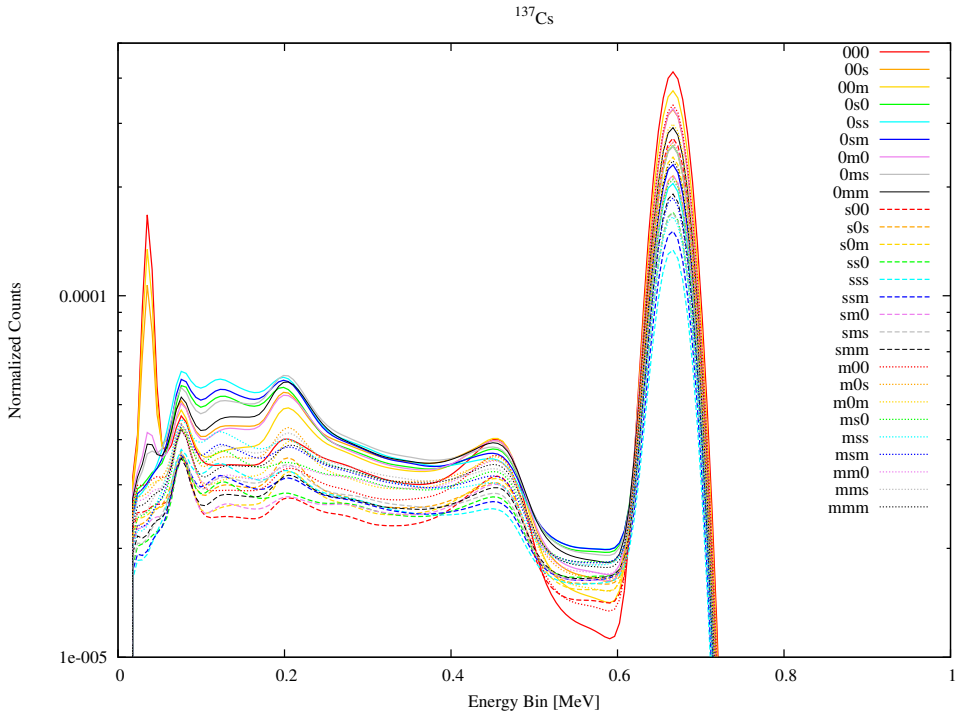

Figure 3.4: Data Set from null to sss Configurations using ^{137}Cs

5% for each energy bin. Figure 3.8 presents the situation where all of the spectra were tightly grouped together at approximately 0.5 MeV. Below this grouping, similar trends can be seen where the distribution was somewhat based on the thickness of the lead shielding. Compared with the second data set using ^{137}Cs, figure 3.9 illustrates that the null condition to the sss configuration for ^{60}Co had a much more organized scenario. This is especially true when considering the spectra below approximately 0.4 MeV.

The spectra generated to create the two data sets using ^{238}U as a radioactive source employed the program GADRAS in generating the distribution of the photon line sources as well as the binned photon groups. GADRAS is a general purpose program used in producing spectra for a wide range of detectors as well as a vast array of source and shielding configurations. It uses a 1D model that combines both ray tracing and SN deterministic transport to rapidly produce a solution a particular problem (Mattingly,

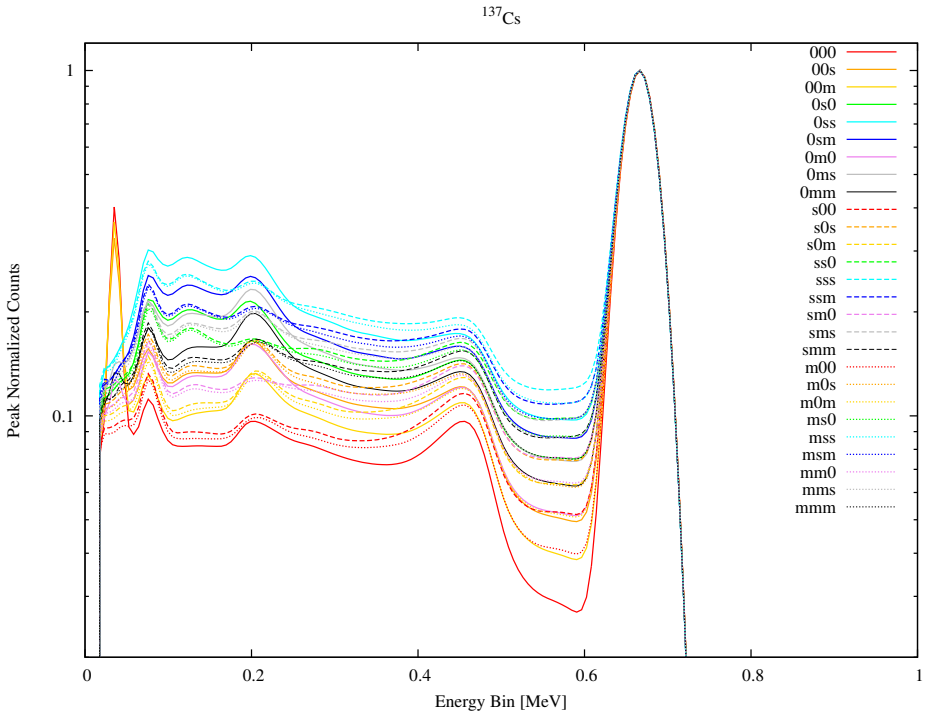

Figure 3.5: Peak Normalized Data Set from null to sss Configurations using ^{137}Cs

2008). Ray tracing is used to calculate the leakage of the source over a finite energy emitted that are neither scattered nor absorbed. The transport model is used to calculate the individual electron, neutron and photon movements as well as the gamma-day and spontaneous fission gamma photon total final profile (Mitchell, Mattingly). Based on the output from GADRAS, the input source definition used to simulate a ^{238}U source in MCNP can be found in the appendix. Due to the energy range of photons being emitted by the source and the low probability of some of those photons, several of the channels experienced relatively large errors despite 1e9 histories being simulated. When the post processing spreading algorithm was executed, the energy bins that produced relative errors larger than 50% were omitted.

Figure 3.10 shows that as with the previous data sets, the same trends that were occurring within the first data set were present. The distinction on the thicknesses of

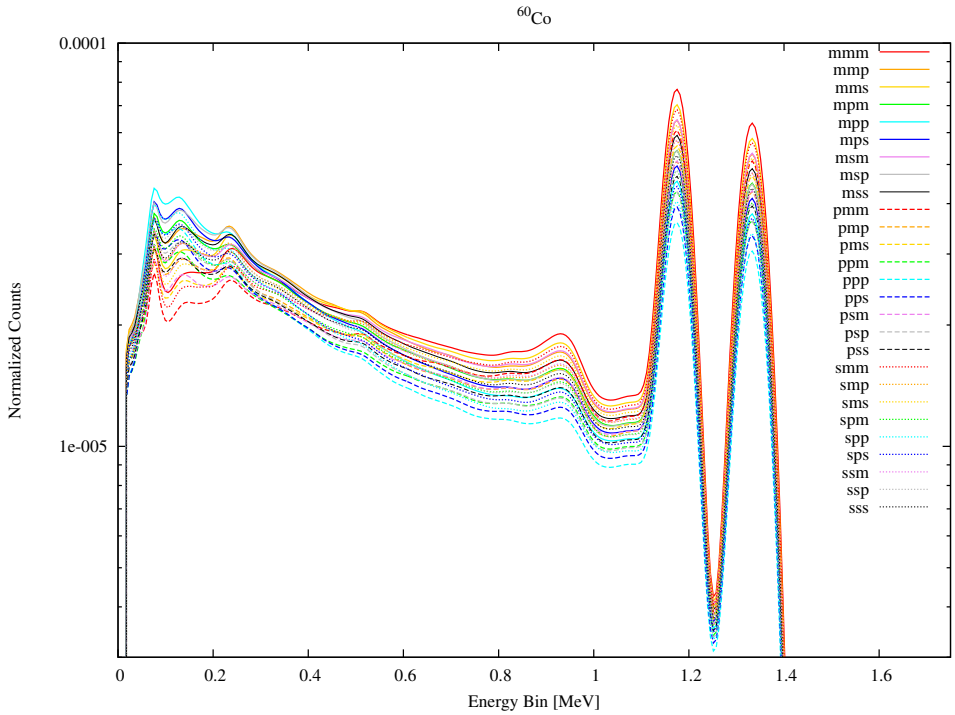

Figure 3.6: Set from mmm to ppp Configurations using ^{60}Co

lead can be made more clearly below approximately 0.3 MeV and became more grouped together above this point. Figure 3.11 was much more difficult to interpret because of the proximity of the entire data set to each other. The same trends were occurring in the order of the aluminum and wood shielding materials but there were few distinctions between each individual spectrum.

The second data set for ^{238}U was created in the exact same manner as the previous data set but with the appropriate shielding thickness. Figure 3.12 clearly shows the most variation between the first data set and the second. This comes from the large distribution of the binned and directly emitted photons from the source as well as the Bremsstrahlung radiation emitted. Figure 3.13 drastically demonstrates the large differences between the two shielding layers of lead and the spectra that have no lead present acting as a shield. This comes from the large intensity of collected photons located at approximately 95 keV

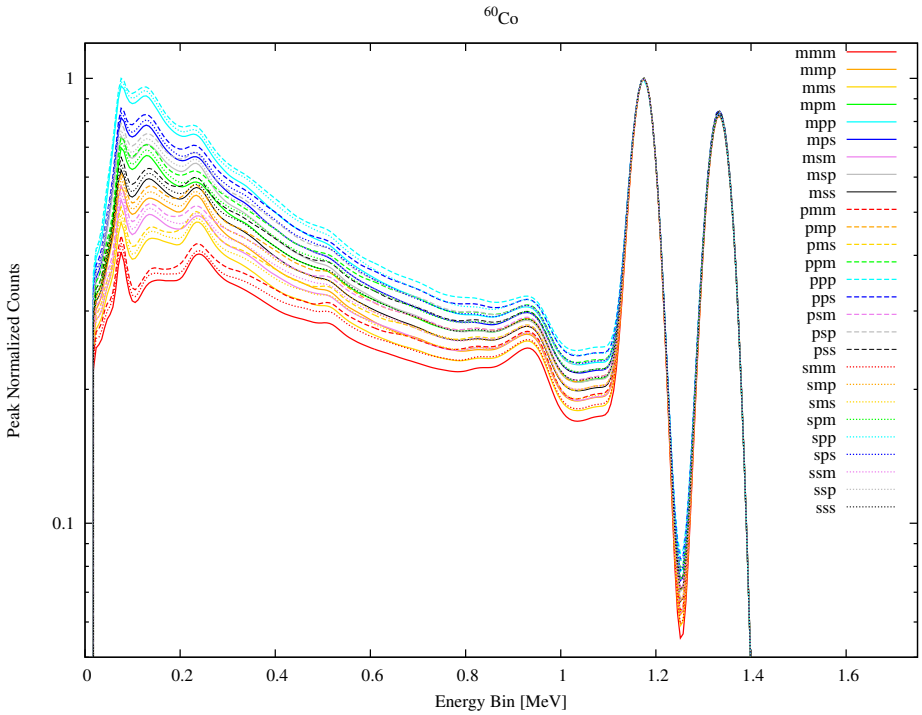

Figure 3.7: Peak Normalized Data Set from mmm to ppp Configurations using ^{60}Co

when the lead shielding was absent.

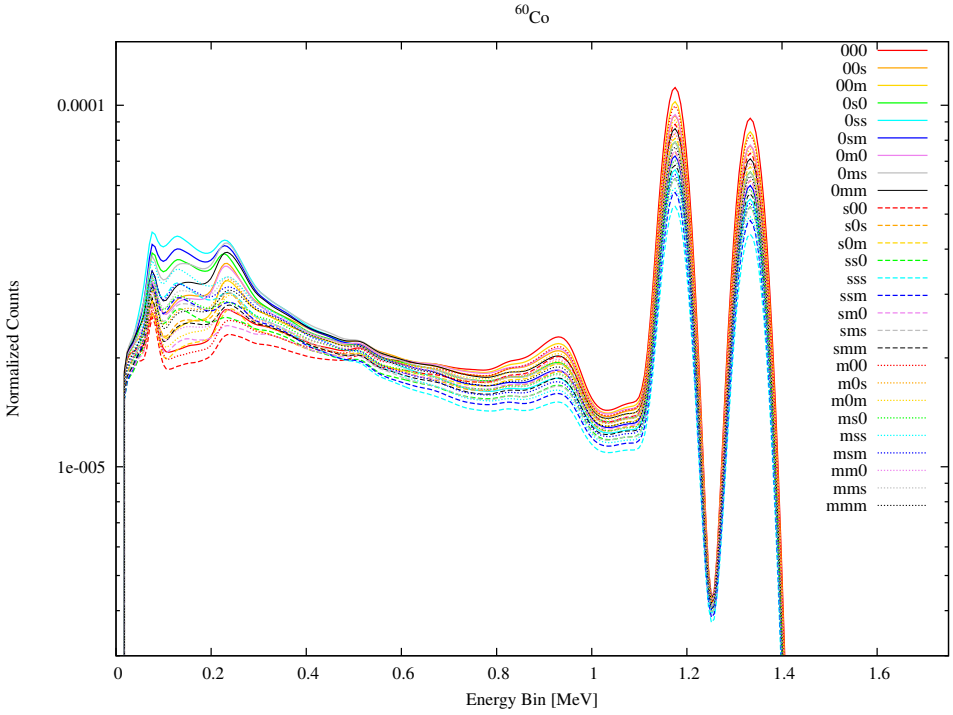

Figure 3.8: Data Set from null to sss Configurations using ^{60}Co

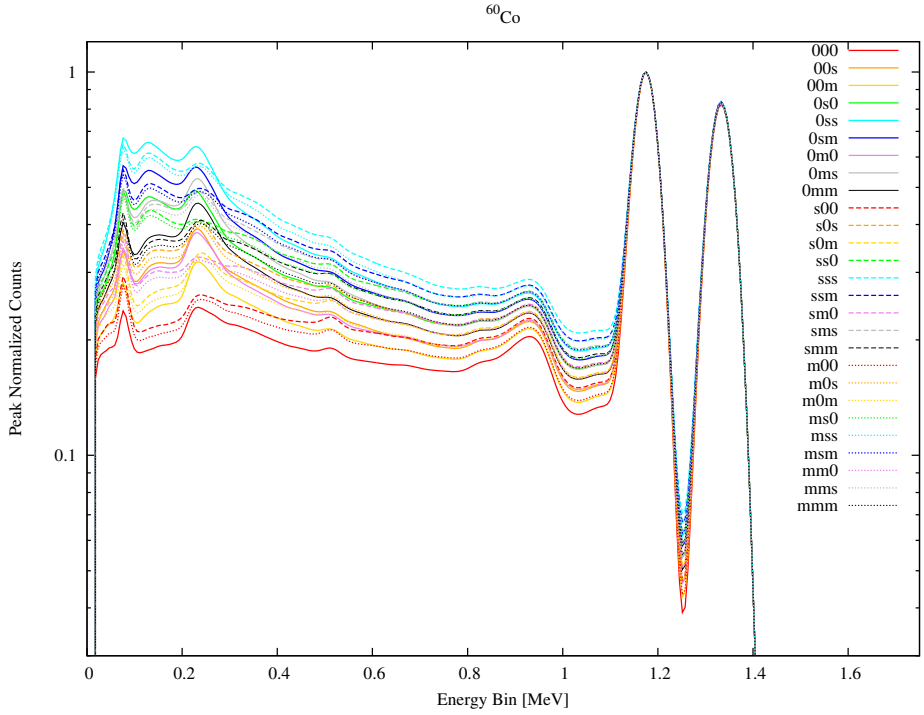

Figure 3.9: Normalized Data Set from null to sss Configurations using ^{60}Co

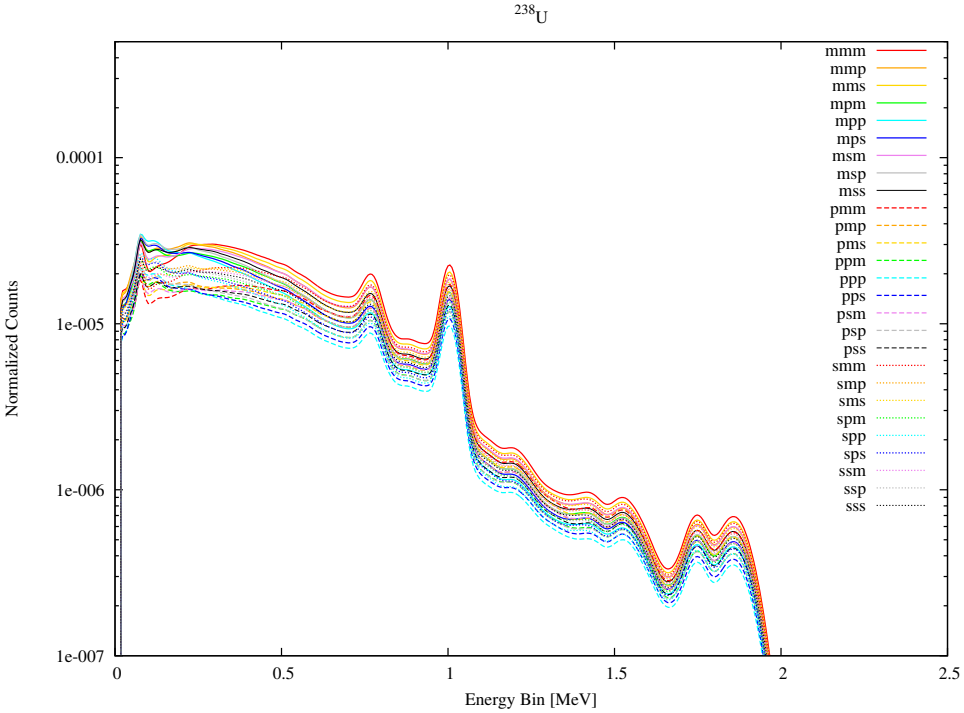

Figure 3.10: Data Set from mmm to ppp Configurations using ^{238}U

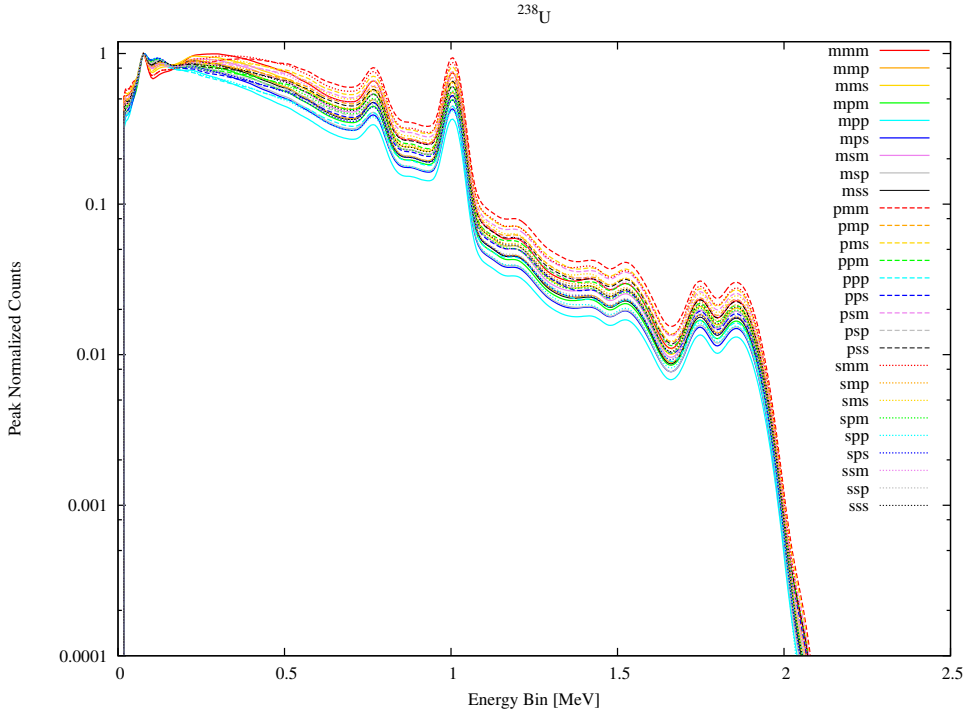

Figure 3.11: Peak Normalized Data Set from mmm to ppp Configurations using ^{238}U

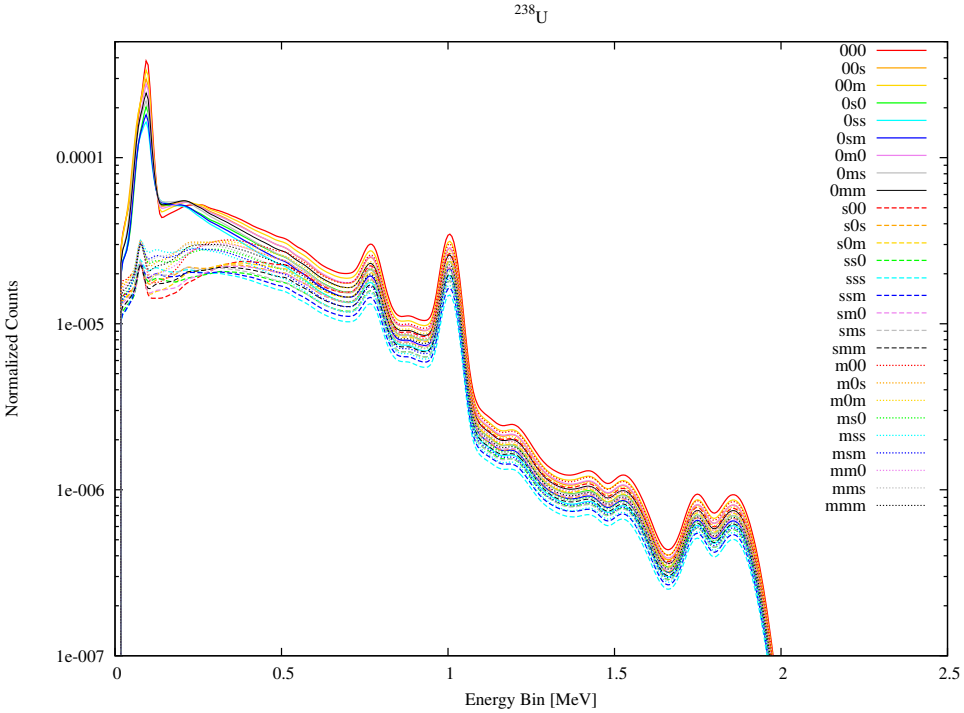

Figure 3.12: Data Set from null to sss Configurations using ^{238}U

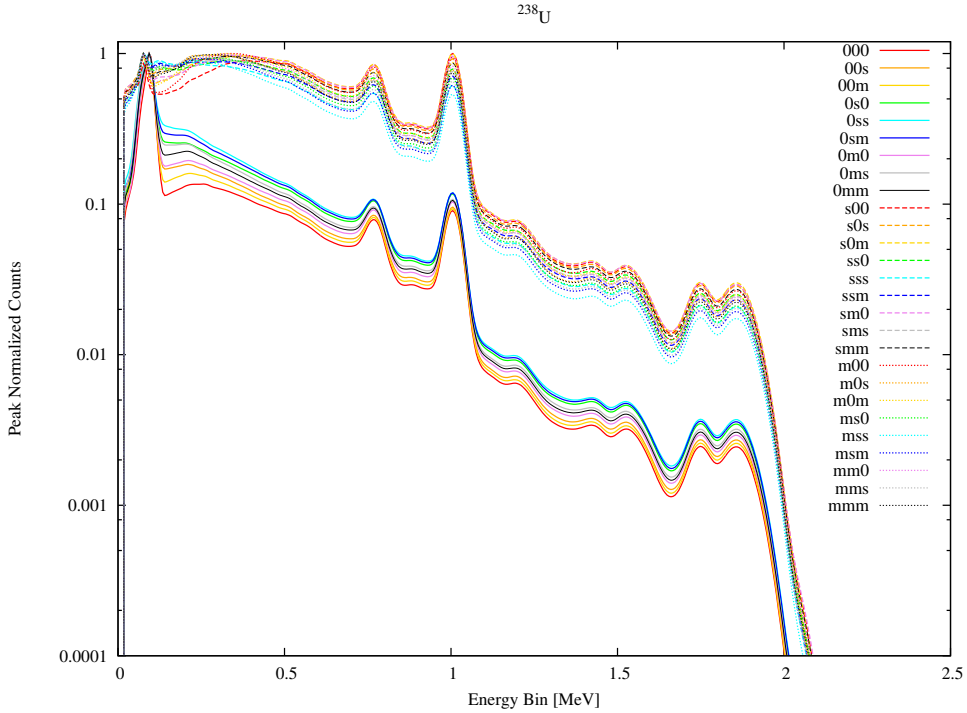

Figure 3.13: Peak Normalized Data Set from null to sss Configurations using ^{238}U

Chapter 4

Tri-Linear Interpolation Model

Now that the libraries have been fully constructed, a specialized model must be constructed for CURMODs use in fitting an input unknown spectrum. Within each data set of libraries, the components that distinguish each spectrum from one another need to be identified. Given that all of the spectra have the same energy bin distribution and bounds, the counts at each channel correspond to the collected photons that have been attenuated or scattered by the specific shielding configurations of lead, aluminum and wood. If the situation where a spectrum was generated with the exact same conditions as one of the libraries, a quick comparison could be made and the shielding material type and thickness could easily be identified. This scenario is very unlikely, so in an attempt to find a solution to the condition where the shielding material thickness within the input spectrum is in-between the thicknesses of the libraries, a model was created that used tri-linear interpolation.

Tri-linear interpolation is an extension of the linear interpolation method but in this instance it extends to three independent variables and approximates the intermediate value within the local axial rectangular prism. In general, consider a unit cube that has

its origin located at the lower left base corner as shown in figure 4.1 where the values at each vertex is denoted by V_{000} through V_{111}.

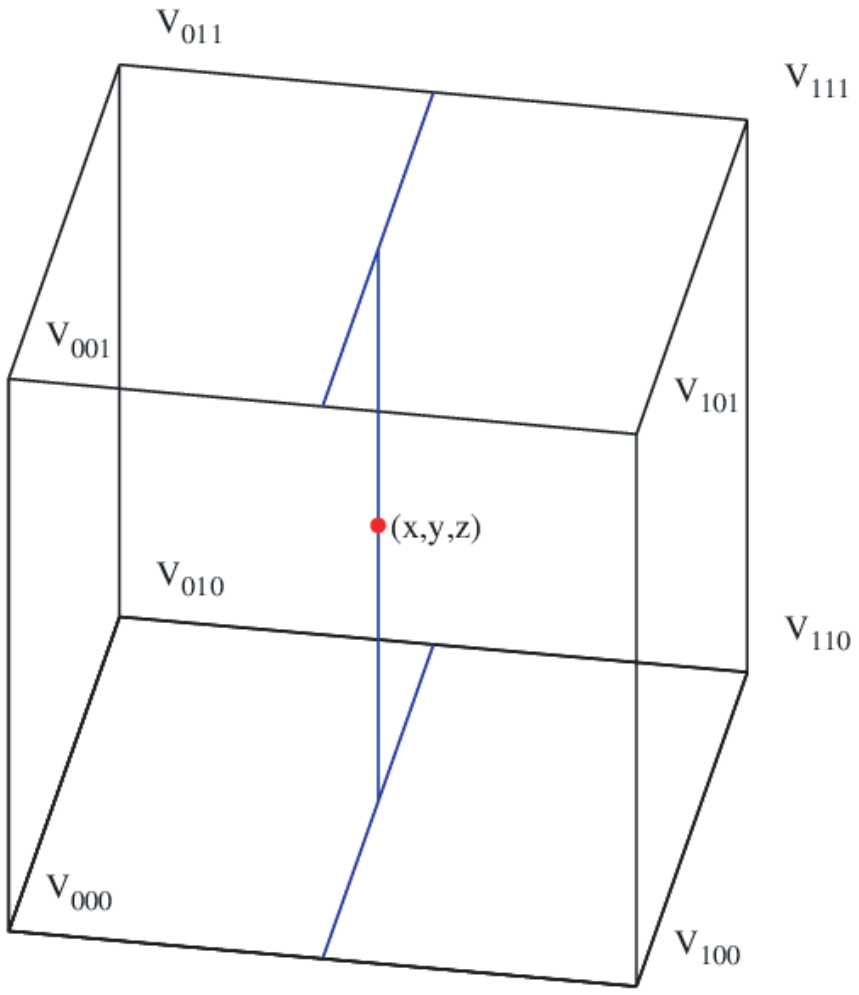

Figure 4.1: Tri-linear Interpolation Method

The resulting equation to solve for the arbitrary point located at x, y, z would then be:

$$
\begin{aligned}
V_{xyz} &= V_{000}(1-x)(1-y)(1-z) + \\
&\quad V_{100}x(1-y)(1-z) + \\
&\quad V_{010}(1-x)y(1-z) + \\
&\quad V_{001}(1-x)(1-y)z + \\
&\quad V_{101}x(1-y)z + \\
&\quad V_{011}(1-x)yz + \\
&\quad V_{110}xy(1-z) + \\
&\quad V_{111}xyz
\end{aligned} \tag{4.1}
$$

The bounding cube will generally not be of unit size nor will it be aligned at the origin but simple translation and scaling of each axis can be used to transform the parameters into and out of the simplified situation.

The tri-linear interpolation used the three independent variables in this problem as the three shielding materials which acted as the direction along which the bounding cube being constructed. The distance along each of the directions corresponded to the thickness of that material. This then dictated that eight of the 27 spectra used in any particular data set were required for this interpolation method to be successful and the location within the defined cube were the thicknesses of the of the input unknown spectrum. The whole data set produces eight separate sectors that were used for material thickness determination. Figure 4.2 shows a physical interpretation of the first data set produced for each radioisotope library where the axes are the materials themselves and the direction along the axes represent the thickness of the corresponding material.

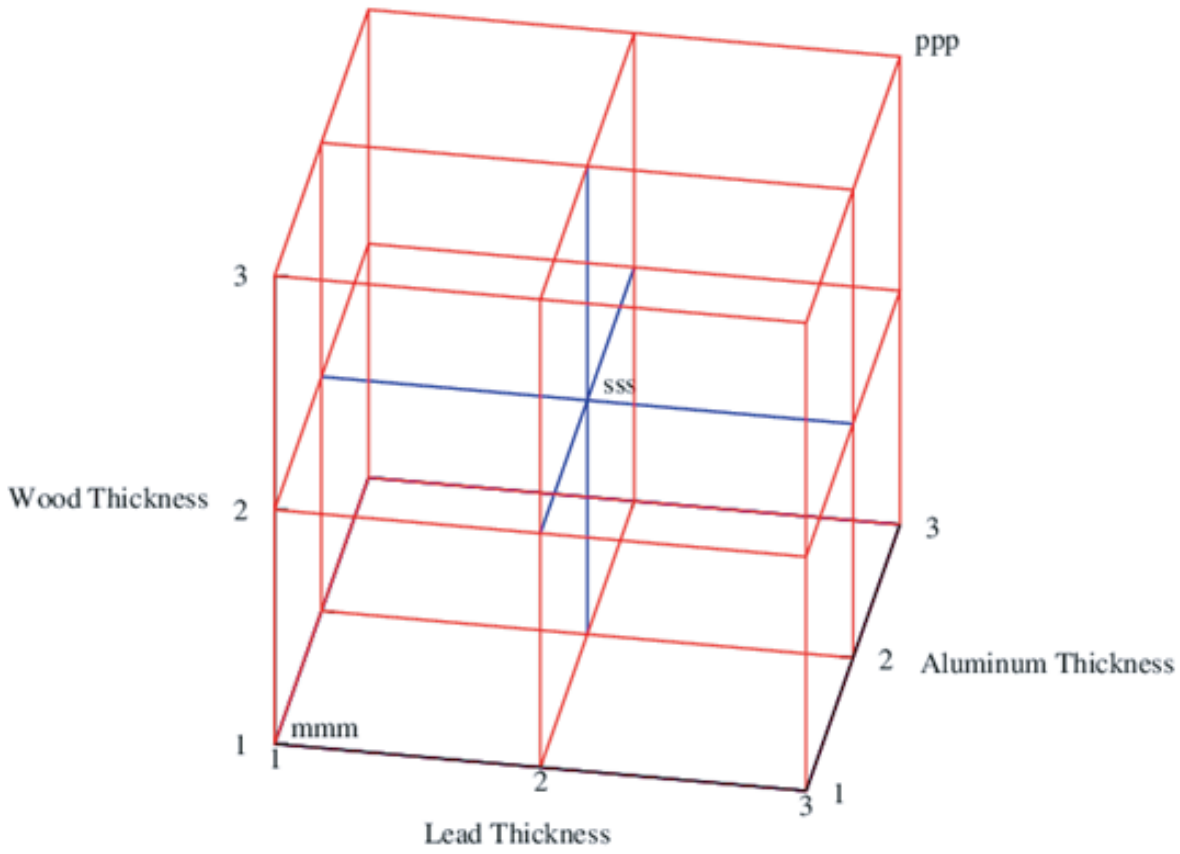

Figure 4.2: Physical Interpretation of the Shielding Materials for Tri-linear Interpolation

Initial guesses are required in CURMOD for the thicknesses of the three materials because these are non-linear parameters and the interpolation was performed at every channel along the spectrum. This scheme also includes a single linear parameter that was used to scale the libraries which can be used to determine the strength of the source.

Chapter 5

The Test Suite

Ensuring that these methods would work properly and that correct thicknesses of the shielding materials would be calculated, spectra were generated with various thickness of the materials in between the previously generated libraries. It was desired to completely test the tri-linear interpolation scheme, so each of the eight sectors produced by both data sets of 27 libraries received a test input spectrum. Considering that there are six complete data sets where each has eight sectors to be tested, a total of 48 input spectra were produced to be considered as unknown to the solving routine. The thicknesses applied in creating these test unknown spectra can be found in table 5.1 and 5.2 that was used to check the tri-linear method for both of the two data set libraries for each radioisotope. The spectra produced by these different shielding material thicknesses can be found in the following figures.

There was a clear distinction between the test Unknown 1 and Unknown 8. This contrasting feature resulted because the sectors that these two spectra resided in were the most drastically different. The spectra produced in the Unknown 2, 3 5, 6, 7 were all somewhat similar along the Compton continuum with the exception of the relative

Table 5.1: Thicknesses of the Test Spectrum for the First Data Set in Centimeters

Unknown 1			Unknown 5		
Pb	m-s	0.2	Pb	s-p	0.51
Al	m-s	1.963	Al	m-s	2.1
Wd	m-s	5	Wd	m-s	6
Unknown 2			Unknown 6		
Pb	m-s	0.3	Pb	s-p	0.5
Al	m-s	2	Al	m-s	1.463
Wd	s-p	8.5	Wd	s-p	9.04
Unknown 3			Unknown 7		
Pb	m-s	0.25	Pb	s-p	0.4
Al	s-p	3.2	Al	s-p	2.6
Wd	m-s	4	Wd	m-s	4.5
Unknown 4			Unknown 8		
Pb	m-s	0.19	Pb	s-p	0.52
Al	s-p	2.8	Al	s-p	3.1
Wd	s-p	10	Wd	s-p	9.4

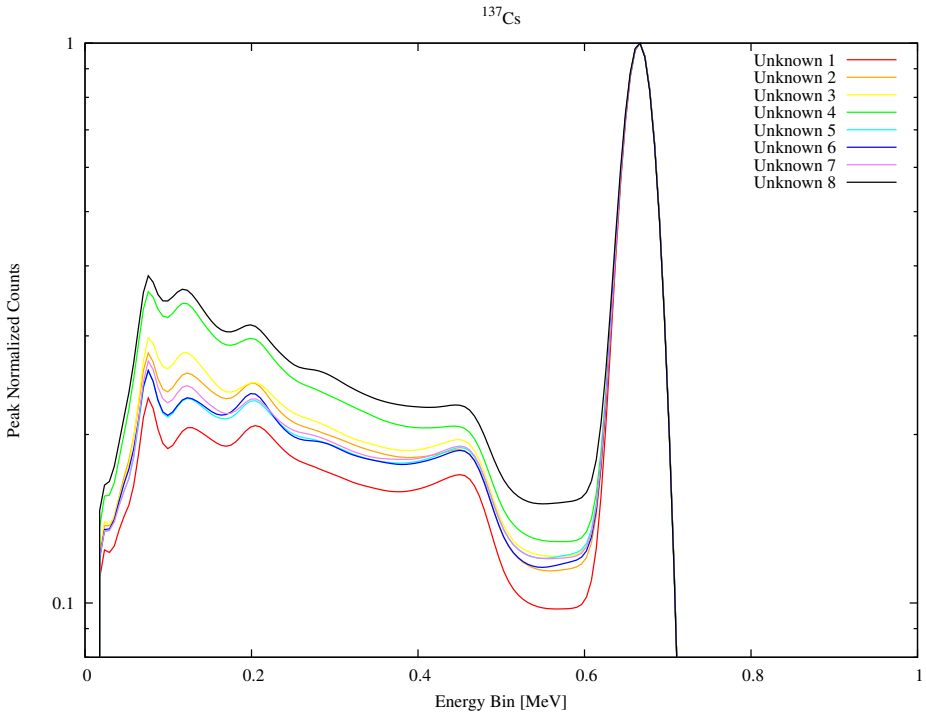

Figure 5.1: Peak Normalized Unknown Test Spectra for the First Data Set Using ^{137}Cs

intensity of the peak produced at approximately 80 keV. Figure 5.2 depicts the same basic trends that occurred in figure 5.1 but in this case the differences were spread out over a larger energy range and there were two primary photo peaks due to ^{60}Co being used.

The spectra produced using ^{238}U in figure 5.3 demonstrated different trends than previously generated with the exception being at approximately 100 keV. These differences stem from the distribution of photon line energies emitted as well as the binned distribution of grouped photons that correspond to the various mass attenuation coefficients that were adjusted for each of the energies.

The unknown input spectra created to test the second data set that ranged from the null condition to the sss configuration used the following shielding thicknesses.

As with the spectra created to test the first data set, these spectra demonstrated the

Table 5.2: Thicknesses of the Test Spectrum for the Second Data Set in Centimeters

Unknown 1			Unknown 5		
Pb	0-m	0.10	Pb	m-s	0.20
Al	0-m	1.00	Al	0-m	0.70
Wd	0-m	2.00	Wd	0-m	3.30
Unknown 2			Unknown 6		
Pb	0-m	0.05	Pb	m-s	0.30
Al	0-m	0.50	Al	0-m	0.30
Wd	m-s	6.80	Wd	m-s	6.00
Unknown 3			Unknown 7		
Pb	0-m	0.15	Pb	m-s	0.25
Al	m-s	1.50	Al	m-s	1.70
Wd	0-m	1.00	Wd	0-m	2.50
Unknown 4			Unknown 8		
Pb	0-m	0.08	Pb	m-s	0.19
Al	m-s	1.80	Al	m-s	2.10
Wd	m-s	4.80	Wd	m-s	7.00

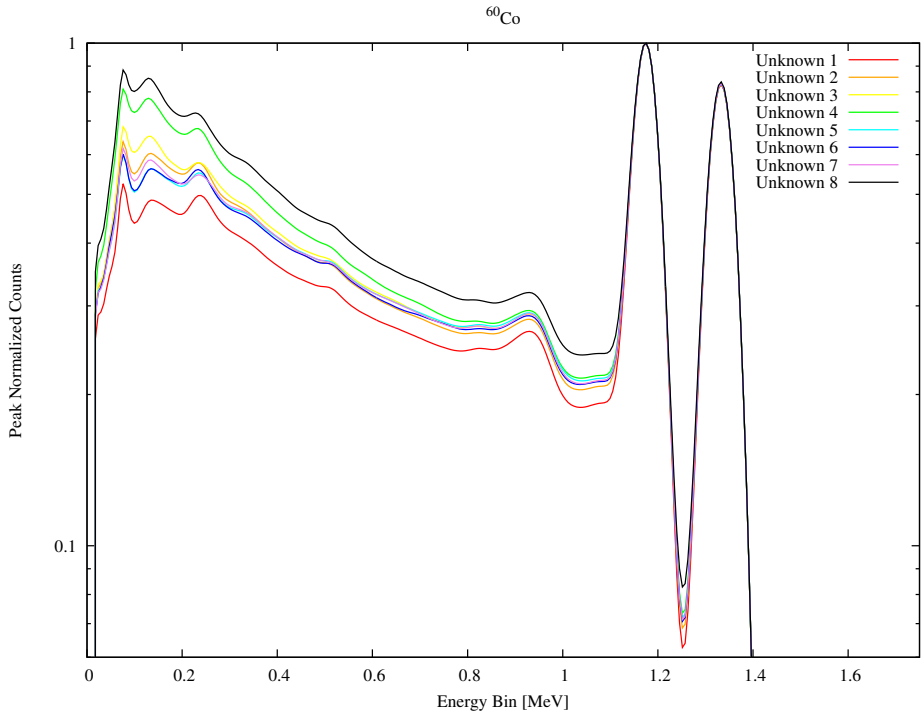

Figure 5.2: Peak Normalized Unknown Test Spectra for the First Data Set Using ^{60}Co

same trends in the order of intensity along the Compton continuum but that the overall count differences were much closer in value for all the spectra created.

Again, figure 5.5 demonstrated the similarities in the order of the intensities along the Compton continuum. Also, the backscatter peak in each spectrum at approximately 0.2 MeV had individual shapes that changed depending on the shielding thicknesses.

The spectra generated for the test suite with ^{238}U demonstrated that the thickness of lead in the shielding configuration helped to dictate the relative intensity of the low energy peak at approximately 75 keV. This could seen in the larger peak experienced from the Unknown 2 configuration where it had the least amount of lead than the other spectra and therefore had the largest discrepancy through the entire spectrum when it had been normalized to its highest peak value.

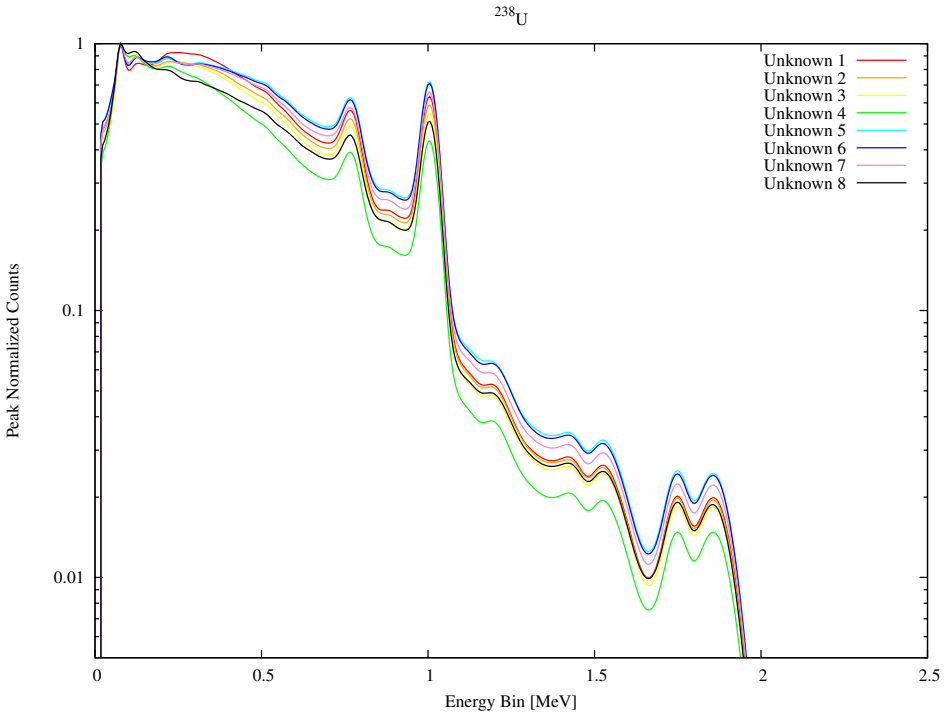

Figure 5.3: Peak Normalized Unknown Test Spectra for the First Data Set Using ^{238}U

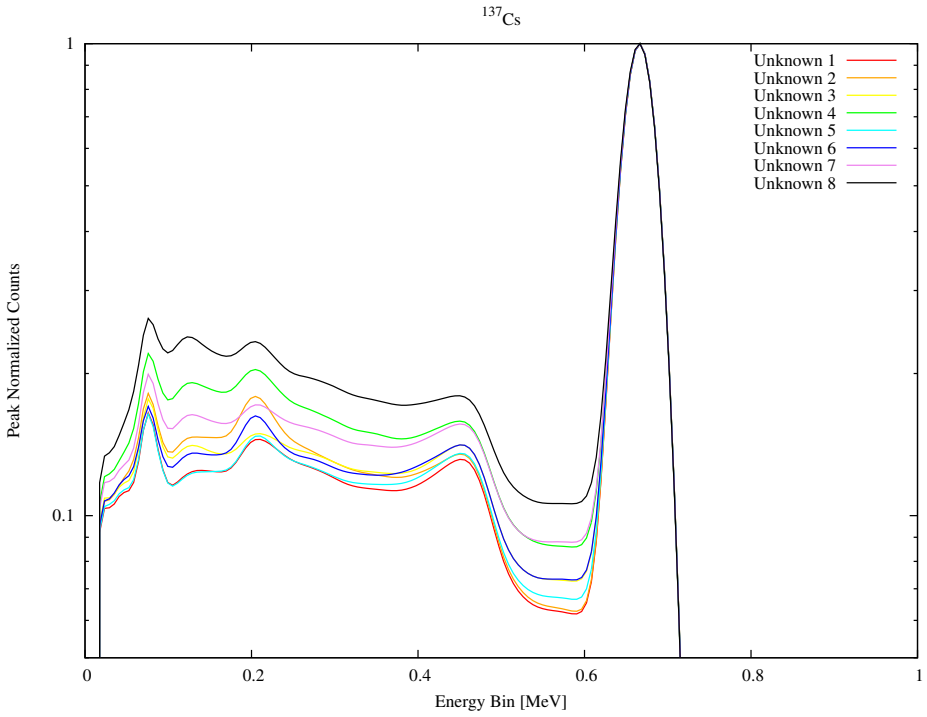

Figure 5.4: Peak Normalized Unknown Test Spectra for the Second Data Set Using ^{137}Cs

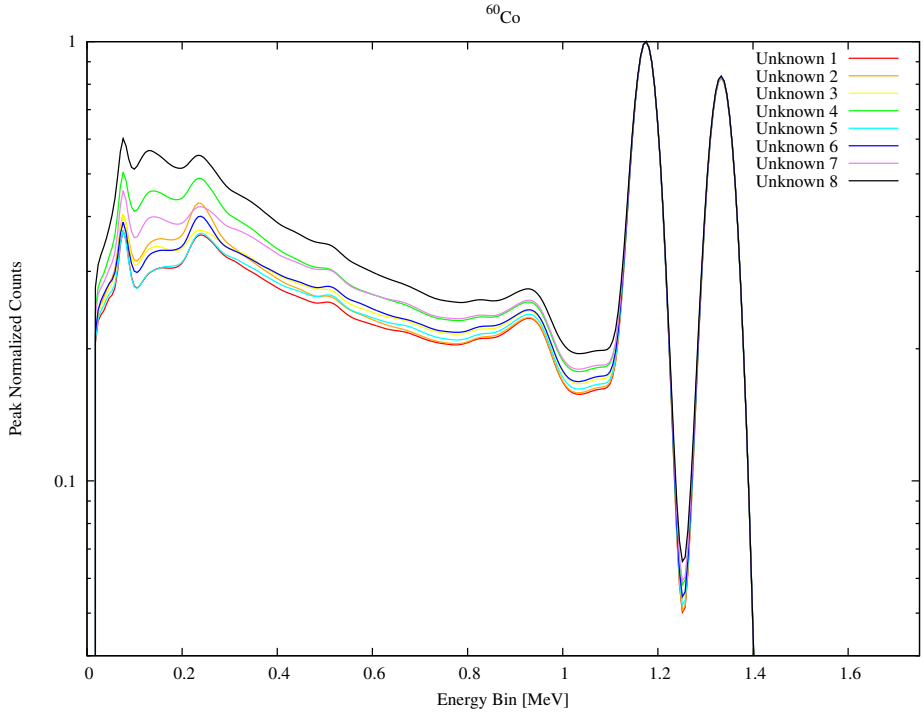

Figure 5.5: Peak Normalized Unknown Test Spectra for the Second Data Set Using ^{60}Co

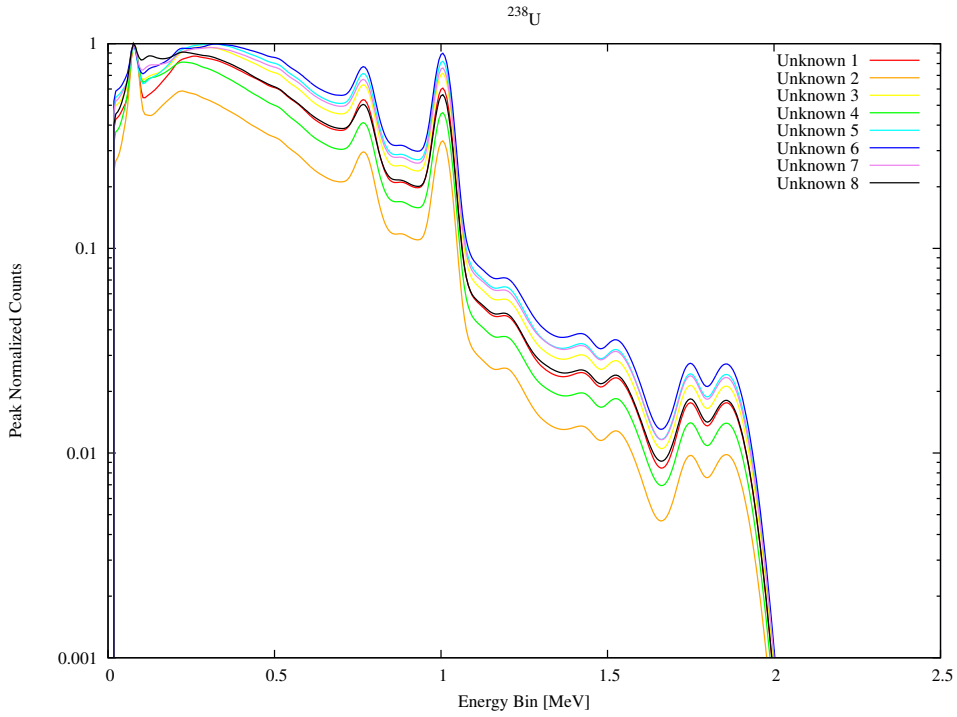

Figure 5.6: Peak Normalized Unknown Test Spectra for the Second Data Set Using ^{238}U

Chapter 6

Testing the Tri-Linear Interpolation Model

Now that two separate complete library data sets have been created for three individual radioisotopes, a model had been generated to make comparisons of an input spectra using tri-linear interpolation and a complete volume of test spectra had been produced to specifically quantify the answers generated, it was only appropriate to perform the tests.

The procedure used to insure the validity of the method was to first choose the input spectrum to test the model. The spectrum produced by MCNP represents a collected yield and as a means to represent a true collected spectrum, all of the counts in each energy bin of the test unknown spectrum were multiplied by 10^8. This scaling factor represented approximately a 4.5 Ci source collected over a 10 minute period but could be adjusted to either increase or decrease the counts collected to better represent any given situation desired. After the scaling, statistical noise was added to the spectrum to further simulate a true collected spectrum. If the value of the data point was less than 25,

Table 6.1: Upper Limit Cutoff Values and their Energies for Each Radioisotope

	Channel	Energy Bin [MeV]
^{137}Cs	103	0.60819
^{60}Co	214	1.2573
^{238}U	159	0.93567

then Poison distributed noise was added which was represented by a whole number. If the data point was larger than the set threshold, Gaussian distributed noise was added which was represented as a continuum of values. At which point the input spectrum was ready to be inspected but before execution, initial guesses for the thicknesses of the materials was required because these are the non-linear parameters within the system. In an ideal condition and as a means to truly test the functionality of the tri-linear interpolation scheme, the initial guesses used were in fact that correct values. This test was designed to ensure the validity of the answers generated rather than the quality of the initial guesses and the adaptability of the method.

The evaluations were limited to only produce a solution from the first channel to a location that was used to help disassociate the high degree of correlation at the full energy photo peaks. This location first considered the highest energy identifying photo peak for the particular radioisotope, its FWHM was then calculated and the upper limit of evaluation was placed twice the FWHM below its corresponding peak. These cutoff points were predetermined and their values can be found in the following table.

The first test considered the data set that used the configurations from mmm to ppp with ^{137}Cs in the lowest possible sector which corresponds to the spectrum Unknown 1 in figure 5.1 with material thicknesses found in table 5.1. A physical interpretation of this sector would be considered as the following:

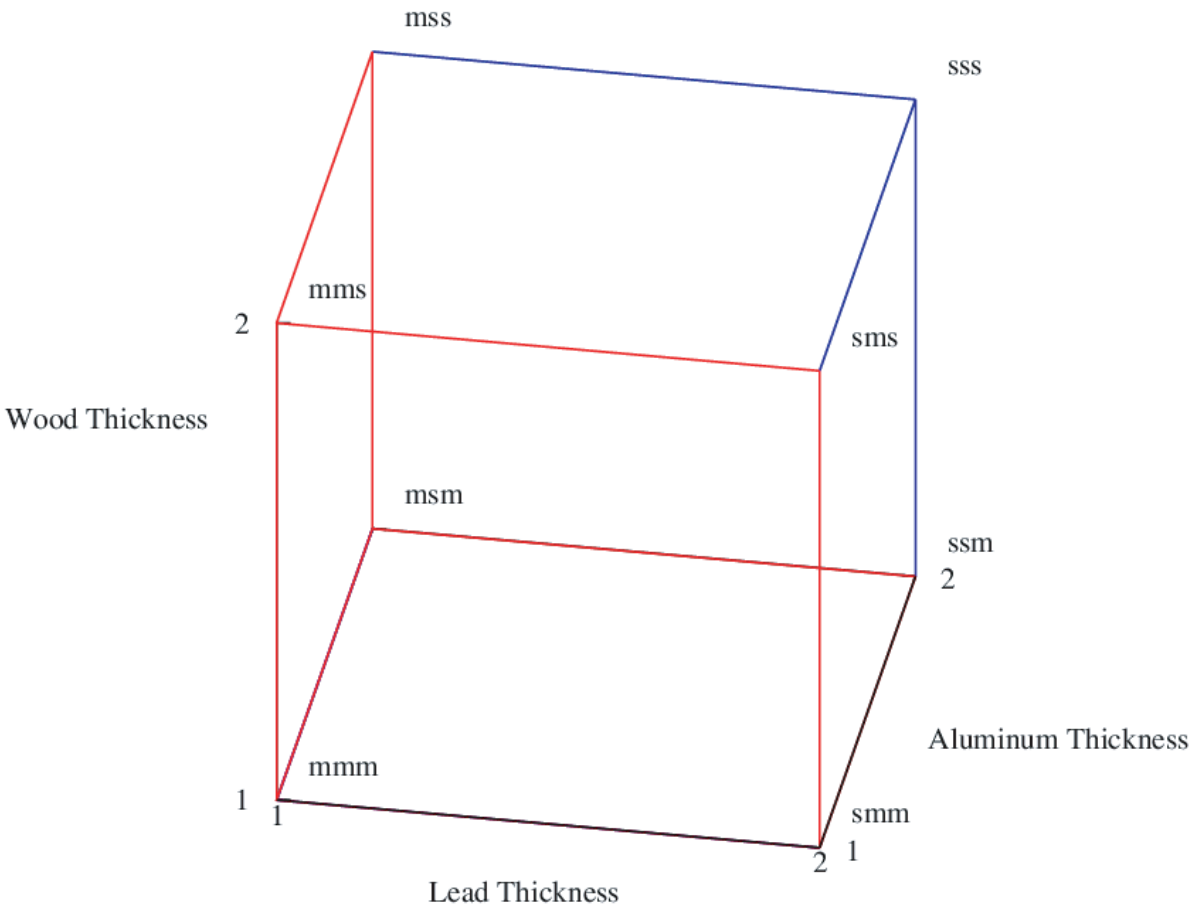

Figure 6.1: Interpretation of the Sector for Unknown 1 in the First Data Set

The example used was located in the lower most shielded condition sector for the first data set library which ranged from the mmm configuration to the sss configuration. The ranges of configurations act as the bounds used in the tri-linear interpolation and the initial guesses act as the location within the cube where the value was desired to be found.

The test was performed for a total of 30 trials with the input unknown spectrum so as a means to produce a range of noise possibilities and a variety of the same basic situation. These found solutions along with their found statistical validity were then averaged and compared with the true solution.

Table 6.2: Thicknesses of the Test Spectrum for the First Data Set in Centimeters

Trial	ChiSqur	Material	Thickness	%Sigma	Material	Thickness	%Sigma	Material	Thickness	%Sigma	Parameter	Value	%Sigma
1	0.8119	Pb=	2.36E-01	1.70E-02	Al=	1.82E+00	4.68E-02	Wood=	5.75E+00	6.82E-02	Linear=	1.03E+08	1.82E-03
2	1.0773	Pb=	1.95E-01	1.60E-02	Al=	2.12E+00	3.37E-02	Wood=	4.16E+00	8.28E-02	Linear=	1.00E+08	1.82E-03
3	1.2044	Pb=	2.00E-01	1.83E-02	Al=	1.90E+00	4.15E-02	Wood=	4.92E+00	7.55E-02	Linear=	1.00E+08	1.82E-03
4	1.2275	Pb=	2.00E-01	1.78E-02	Al=	1.97E+00	3.95E-02	Wood=	4.85E+00	7.58E-02	Linear=	1.00E+08	1.82E-03
5	0.9771	Pb=	1.97E-01	1.72E-02	Al=	2.02E+00	3.74E-02	Wood=	4.52E+00	7.96E-02	Linear=	1.00E+08	1.81E-03
6	1.0629	Pb=	1.96E-01	1.68E-02	Al=	2.06E+00	3.61E-02	Wood=	4.48E+00	7.95E-02	Linear=	9.99E+07	1.82E-03
7	0.9421	Pb=	2.07E-01	1.73E-02	Al=	1.95E+00	4.01E-02	Wood=	4.87E+00	7.59E-02	Linear=	1.01E+08	1.81E-03
8	1.13	Pb=	1.98E-01	1.78E-02	Al=	1.95E+00	3.93E-02	Wood=	4.55E+00	8.01E-02	Linear=	1.00E+08	1.82E-03
9	1.0343	Pb=	2.00E-01	1.74E-02	Al=	2.02E+00	3.80E-02	Wood=	4.91E+00	7.41E-02	Linear=	1.00E+08	1.82E-03
10	1.0009	Pb=	1.95E-01	1.63E-02	Al=	2.11E+00	3.43E-02	Wood=	4.24E+00	8.19E-02	Linear=	1.00E+08	1.82E-03
11	0.9457	Pb=	1.96E-01	1.60E-02	Al=	2.14E+00	3.36E-02	Wood=	4.31E+00	8.03E-02	Linear=	1.00E+08	1.82E-03
12	1.3636	Pb=	1.97E-01	1.71E-02	Al=	2.02E+00	3.72E-02	Wood=	4.53E+00	7.91E-02	Linear=	1.00E+08	1.82E-03
13	1.082	Pb=	2.00E-01	1.81E-02	Al=	1.93E+00	4.06E-02	Wood=	4.88E+00	7.58E-02	Linear=	9.99E+07	1.82E-03
14	1.0627	Pb=	2.02E-01	1.81E-02	Al=	1.94E+00	4.08E-02	Wood=	5.10E+00	7.30E-02	Linear=	1.00E+08	1.82E-03
15	1.0487	Pb=	2.02E-01	1.67E-02	Al=	2.04E+00	3.71E-02	Wood=	4.74E+00	7.61E-02	Linear=	1.01E+08	1.82E-03
16	0.9312	Pb=	1.97E-01	1.69E-02	Al=	2.06E+00	3.62E-02	Wood=	4.51E+00	7.91E-02	Linear=	1.00E+08	1.81E-03
17	1.1354	Pb=	2.00E-01	1.81E-02	Al=	1.93E+00	4.05E-02	Wood=	4.88E+00	7.57E-02	Linear=	1.00E+08	1.82E-03
18	1.5948	Pb=	1.96E-01	1.68E-02	Al=	2.08E+00	3.57E-02	Wood=	4.45E+00	7.98E-02	Linear=	1.00E+08	1.82E-03
19	1.0855	Pb=	2.03E-01	1.87E-02	Al=	1.88E+00	4.30E-02	Wood=	5.32E+00	7.11E-02	Linear=	1.00E+08	1.81E-03
20	1.0101	Pb=	1.97E-01	1.66E-02	Al=	2.08E+00	3.56E-02	Wood=	4.52E+00	7.83E-02	Linear=	1.00E+08	1.82E-03
21	1.2601	Pb=	1.93E-01	1.52E-02	Al=	2.21E+00	3.12E-02	Wood=	3.89E+00	8.60E-02	Linear=	1.00E+08	1.82E-03
22	0.913	Pb=	1.98E-01	1.72E-02	Al=	2.02E+00	3.74E-02	Wood=	4.67E+00	7.70E-02	Linear=	1.00E+08	1.81E-03
23	1.1448	Pb=	1.95E-01	1.67E-02	Al=	2.04E+00	3.58E-02	Wood=	4.13E+00	8.51E-02	Linear=	1.00E+08	1.82E-03
24	1.192	Pb=	2.02E-01	1.86E-02	Al=	1.89E+00	4.24E-02	Wood=	5.19E+00	7.25E-02	Linear=	1.01E+08	1.81E-03
25	0.9775	Pb=	2.05E-01	1.95E-02	Al=	1.80E+00	4.61E-02	Wood=	5.63E+00	6.84E-02	Linear=	1.00E+08	1.82E-03
26	1.1092	Pb=	1.99E-01	1.77E-02	Al=	1.98E+00	3.90E-02	Wood=	4.88E+00	7.49E-02	Linear=	1.00E+08	1.81E-03
27	1.0374	Pb=	1.99E-01	1.78E-02	Al=	1.96E+00	3.95E-02	Wood=	4.85E+00	7.58E-02	Linear=	1.00E+08	1.82E-03
28	0.7799	Pb=	2.02E-01	1.81E-02	Al=	1.95E+00	4.06E-02	Wood=	5.23E+00	7.13E-02	Linear=	1.00E+08	1.82E-03
29	1.1755	Pb=	1.99E-01	1.80E-02	Al=	1.93E+00	4.01E-02	Wood=	4.75E+00	7.72E-02	Linear=	1.00E+08	1.81E-03
30	0.8233	Pb=	2.02E-01	1.85E-02	Al=	1.88E+00	4.24E-02	Wood=	5.15E+00	7.29E-02	Linear=	1.00E+08	1.82E-03
AVERAGE=	1.07E+00		2.00E-01	1.74E-02		1.99E+00	3.87E-02		4.76E+00	7.68E-02		1.00E+08	1.82E-03

Table 6.2 demonstrates 30 individual solutions that were produced. Each of the answers produced a χ^2 that represents a valid solution to the input unknown problem and based on the averages generated, the found thicknesses for lead and aluminum were very close to the exact answer of 0.2 and 1.963 cm respectively. The value found for wood was within one standard deviation to the true solution of 5 cm. Also, the linear fitting parameter was very close to the true value with very good statistical confidence. Figure 6.2 illustrates the found solution for the 30^{th} trial in the previous table.

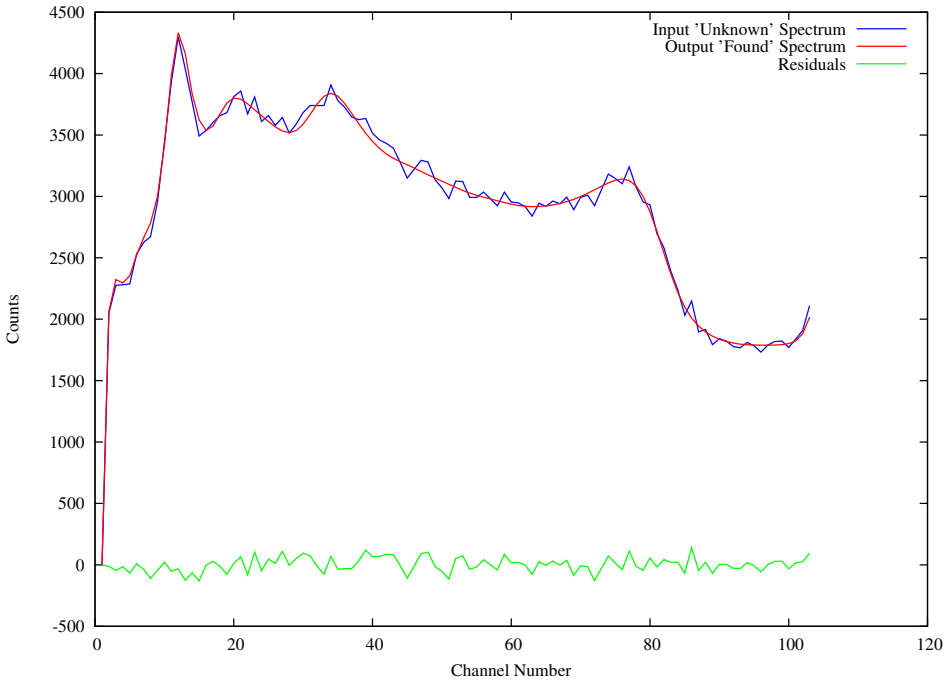

Figure 6.2: Tri-Linear Fit for the 30^{th} Trial in Table 6.2

The found results that fit the input spectrum produced a solution that appears upon the statistical and visual inspection as a good approximation. The average of the residuals generated by this fit was 1.31 which also demonstrated a relatively good fit. This procedure was repeated for each of the 24 test unknown spectra using the first data set

of libraries.

Table 6.3: Averages of 30 Trials with the First Data Set Using ^{137}Cs

	χ^2	Pb TRUE	Pb Meas.	Pb σ(%)	Al TRUE	Al Meas.	Al σ(%)	Wood TRUE	Wood Meas.	Wood σ(%)	Amount Meas.	Amount σ(%)
unk1	1.071	0.20	0.20	1.74	1.96	1.99	3.87	5.00	4.76	7.68	1.00E+08	0.18
unk2	1.024	0.30	0.29	1.37	2.00	2.14	4.60	8.50	7.92	4.82	9.99E+07	0.19
unk3	1.038	0.25	0.25	1.39	3.20	3.19	2.26	4.00	4.06	9.15	9.99E+07	0.19
unk4	1.031	0.19	0.19	3.53	2.80	2.85	4.07	10.00	9.89	4.69	1.00E+08	0.18
unk5	1.072	0.51	0.51	0.87	2.10	2.00	5.29	6.00	6.29	7.68	9.98E+07	0.21
unk6	1.093	0.50	0.49	1.52	1.46	1.48	11.42	9.04	8.92	6.91	9.94E+07	0.21
unk7	1.020	0.40	0.40	1.27	2.60	2.60	3.72	4.50	4.44	10.33	1.00E+08	0.20
unk8	1.079	0.52	0.52	1.15	3.10	3.05	4.27	9.40	9.77	5.50	9.93E+07	0.22
Averages σ(%)				1.60			4.94			7.10		0.20
Absolute Average Error			2.47E-03			5.02E-02			2.28E-01		2.86E+05	

Table 6.4: Averages of 30 Trials with the First Data Set Using ^{60}Co

	χ^2	Pb TRUE	Pb Meas.	Pb σ(%)	Al TRUE	Al Meas.	Al σ(%)	Wood TRUE	Wood Meas.	Wood σ(%)	Amount Meas.	Amount σ(%)
unk1	1.023	0.20	0.21	3.70	1.96	1.85	6.04	5.00	5.58	9.20	1.00E+08	0.15
unk2	1.021	0.30	0.29	2.67	2.00	2.13	5.09	8.50	7.98	5.99	1.00E+08	0.15
unk3	1.016	0.25	0.25	2.39	3.20	3.19	2.64	4.00	4.13	10.32	1.00E+08	0.15
unk4	1.016	0.19	0.19	5.61	2.80	2.77	4.69	10.00	10.20	5.27	1.00E+08	0.15
unk5	1.043	0.51	0.51	1.31	2.10	2.08	5.12	6.00	6.05	8.10	1.00E+08	0.16
unk6	1.058	0.50	0.50	2.19	1.46	1.53	10.74	9.04	8.79	7.31	1.00E+08	0.15
unk7	1.017	0.40	0.41	1.68	2.60	2.54	3.55	4.50	4.79	8.53	1.00E+08	0.15
unk8	1.066	0.52	0.52	1.74	3.10	3.15	4.09	9.40	9.22	6.17	1.00E+08	0.16
Averages σ(%)				2.66			5.24			7.61		0.15
Absolute Average Error			4.73E-03			5.95E-02			2.75E-01		1.53E+05	

Table 6.5: Averages of 30 Trials with the First Data Set Using ^{238}U

	χ^2	Pb TRUE	Pb Meas.	Pb σ(%)	Al TRUE	Al Meas.	Al σ(%)	Wood TRUE	Wood Meas.	Wood σ(%)	Amount Meas.	Amount σ(%)
unk1	1.042	0.20	0.20	2.06	1.96	2.00	5.79	5.00	4.64	12.61	9.99E+07	0.18
unk2	1.023	0.30	0.31	1.36	2.00	1.90	6.32	8.50	8.71	6.33	9.91E+07	0.20
unk3	1.015	0.25	0.26	1.54	3.20	3.17	3.29	4.00	3.87	14.28	9.92E+07	0.20
unk4	1.080	0.19	0.19	3.56	2.80	2.82	4.99	10.00	9.99	6.04	9.97E+07	0.19
unk5	1.075	0.51	0.51	1.02	2.10	2.06	7.08	6.00	6.10	11.58	9.96E+07	0.22
unk6	1.043	0.50	0.50	1.35	1.46	1.44	12.04	9.04	9.03	7.76	9.93E+07	0.22
unk7	1.032	0.40	0.40	1.44	2.60	2.57	5.02	4.50	4.56	12.95	9.96E+07	0.21
unk8	1.012	0.52	0.51	1.05	3.10	3.25	3.90	9.40	8.79	6.93	9.98E+07	0.23
Averages σ(%)				1.67			6.05			9.81		0.21
Absolute Average Error			3.52E-03			5.35E-02			1.85E-01		4.86E+05	

The solutions for the first data set proved as an overall success. The measured thicknesses for lead were extremely close with the largest discrepancy between the true and calculated value as 0.01 cm. Aluminum was also relatively close in value with the largest difference being 0.15 cm and wood with the largest inexact value off by 0.61 cm. These differences were experienced using ^{238}U and the spectrum Unknown 8 which can be attributed to the shielding material thicknesses of this test being close to the bounding edges of the tri-linear interpolation. Also, the variations in the shielding present have significantly distorted the spectra for ^{238}U from the large distribution and probabilities of the emitted radiation. With all of these distortions being present, the linear fitting amount is again close to the true value of 1E8 and a good representation of the activity for the found source used could be made. Its associated error is also small which denotes the overall confidence in the found solution for this linear parameter.

As before, 30 trials of the same test unknown spectra were performed and then averaged but in the following tables, the second data set of libraries was used and therefore generated another set of 24 averages with statistical values. These configurations ranged from the null condition to the sss configuration.

Table 6.6: Averages of 30 Trials with the Second Data Set Using ^{137}Cs

	χ^2	Pb TRUE	Pb Meas.	Pb σ(%)	Al TRUE	Al Meas.	Al σ(%)	Wood TRUE	Wood Meas.	Wood σ(%)	Amount Meas.	Amount σ(%)
unk1	1.505	0.10	0.00	224.34	1.00	0.48	8.61	2.00	0.08	251.98	1.06E+08	0.18
unk2	2.878	0.05	0.09	1.10	0.50	0.00	NaN	6.80	3.67	2.30	1.03E+08	0.17
unk3	17.552	0.15	0.10	10.35	1.50	1.18	0.50	1.00	0.91	17.51	9.03E+07	0.18
unk4	1.409	0.08	0.04	5.03	1.80	1.74	2.36	4.80	1.58	7.73	1.05E+08	0.17
unk5	1.278	0.20	0.25	1.26	0.70	0.55	8.59	3.30	0.10	13.64	1.04E+08	0.18
unk6	1.134	0.30	0.29	1.11	0.30	0.59	10.71	6.00	4.86	4.56	1.00E+08	0.19
unk7	1.056	0.25	0.27	1.06	1.70	1.60	2.68	2.50	0.87	27.14	1.02E+08	0.19
unk8	1.081	0.19	0.19	2.02	2.10	2.09	3.85	7.00	6.81	5.52	1.00E+08	0.18
Averages σ(%)				30.78			5.33			41.30		0.18
Absolute Average Error			0.04			0.24			1.82		6.14E+05	

Table 6.6 demonstrates very poor solutions for all of the spectra except for Unknown 8. The primary reason for these drastic discrepancies between the first and second data set arrangement solutions stem from the lack of shielding experienced. Given the low energy photons were not attenuated as much, the collected spectra differ quite largely and these differences cause the tri-linear interpolation model to achieve a less than desirable solution and these differences can be seen in the library used in figures 3.4 and 3.5. The poor results for each of the shielding material thicknesses are shown in the averages for the percent of standard deviations having large values from the inability to resolve the parameters. One answer to help resolve this issue was to ignore the low energy portion of the libraries and collected spectra and in this case that threshold was placed at the 13^{th} channel which was at approximately 80keV.

Table 6.7: Averages of 30 Trials with the Second Data Set Using ^{137}Cs Over a Reduced Range

	χ^2	Pb TRUE	Pb Meas.	Pb σ(%)	Al TRUE	Al Meas.	Al σ(%)	Wood TRUE	Wood Meas.	Wood σ(%)	Amount Meas.	Amount σ(%)
unk1	1.281	0.10	0.01	62.00	1.00	0.47	10.37	2.00	0.41	90.02	1.06E+08	0.19
unk2	1.290	0.05	0.09	3.18	0.50	0.47	13.77	6.80	5.90	5.52	1.05E+08	0.18
unk3	1.353	0.15	0.00	62.46	1.50	0.00	NaN	1.00	1.71	8.24	1.02E+08	0.19
unk4	1.084	0.08	0.04	15.66	1.80	1.56	8.41	4.80	4.95	32.08	1.04E+08	0.20
unk5	1.151	0.20	0.24	1.67	0.70	0.48	10.50	3.30	0.41	61.19	1.04E+08	0.20
unk6	1.002	0.30	0.29	1.20	0.30	0.59	11.90	6.00	4.82	4.63	9.99E+07	0.20
unk7	0.957	0.25	0.27	1.28	1.70	1.59	2.80	2.50	0.91	28.92	1.02E+08	0.20
unk8	0.879	0.19	0.19	2.09	2.10	2.13	4.14	7.00	6.66	6.0	3 1.00E+08	0.19
Averages σ(%)				18.69			8.84			29.58		0.19
Absolute Average Error			0.05			0.37			1.17		6.41E+05	

Reducing the range over which the tri-linear interpolation does assist in choosing the correct values in most cases. The channels over which the evaluation occurs could be adjusted depending on the radioisotope and the total amount of collected photons. In general, the tri-linear approach does not produce reputable solutions when there is little shielding material present in the spectrum. However, the solutions generated that produce a χ^2 close to 1 place the thicknesses of the material within the appropriate bounds of the library which still holds useful information with the only exception of Unknown 3 in the previous table.

Table 6.8: Averages of 30 Trials with the Second Data Set Using ^{60}Co Over the Full Range

	χ^2	Pb TRUE	Pb Meas.	Pb σ(%)	Al TRUE	Al Meas.	Al σ(%)	Wood TRUE	Wood Meas.	Wood σ(%)	Amount Meas.	Amount σ(%)
unk1	1.076	0.10	0.02	19.21	1.00	0.43	14.75	2.00	0.37	101.26	1.02E+08	0.14
unk2	1.128	0.05	0.10	3.56	0.50	0.21	49.42	6.80	4.43	11.23	1.02E+08	0.14
unk3	1.033	0.15	0.01	127.76	1.50	1.36	2.94	1.00	1.90	11.11	1.01E+08	0.14
unk4	1.041	0.08	0.04	9.49	1.80	1.45	5.51	4.80	6.11	6.77	1.01E+08	0.14
unk5	1.095	0.20	0.22	2.36	0.70	0.50	11.90	3.30	0.16	603.07	1.01E+08	0.14
unk6	1.063	0.30	0.32	2.50	0.30	0.72	14.15	6.00	5.42	6.81	1.01E+08	0.15
unk7	1.052	0.25	0.27	1.57	1.70	1.58	2.79	2.50	0.51	49.90	1.01E+08	0.15
unk8	1.007	0.19	0.19	2.74	2.10	2.11	2.98	7.00	7.00	4.35	1.00E+08	0.15
Averages σ(%)				21.15			13.06			99.31		0.14
Absolute Average Error			0.05			0.37			1.17		6.41E+05	

The results for the second data set for ^{60}Co were better in general than the results found for ^{137}Cs. This was because with this new source, there were no lower energies being emitted and therefore the differences between each of the libraries diminished. Since the highest energy was being used to locate the upper limit of the evaluations, the second full energy peak was used in the fitting routine which gives a higher degree of correlation than if just the portion of the spectrum that had the Compton continuum was considered. Also, the total number of channels considered was larger than previously used.

Table 6.9: Averages of 30 Trials with the Second Data Set Using ^{238}U Over a Limited Range

	χ^2	Pb TRUE	Pb Meas.	Pb σ(%)	Al TRUE	Al Meas.	Al σ(%)	Wood TRUE	Wood Meas.	Wood σ(%)	Amount Meas.	Amount σ(%)
unk1	1.327	0.10	0.10	0.86	1.00	0.78	3.36	2.00	3.48	4.40	8.80E+07	0.18
unk2	1.069	0.05	0.10	1.43	0.50	0.09	738.51	6.80	6.32	41.08	1.04E+08	0.18
unk3	1.140	0.15	0.00	38.82	1.50	1.06	11.35	1.00	7.15	9.04	1.06E+08	0.19
unk4	1.186	0.08	0.07	8.39	1.80	1.56	20.84	4.80	6.83	27.35	1.02E+08	0.19
unk5	0.833	0.20	0.31	1.20	0.70	0.00	81726.35	3.30	1.40	39.00	1.05E+08	0.20
unk6	0.830	0.30	0.25	1.07	0.30	1.07	8.98	6.00	5.14	7.90	9.48E+07	0.21
unk7	0.807	0.25	0.28	2.69	1.70	1.38	13.61	2.50	2.33	41.97	1.02E+08	0.21
unk8	0.813	0.19	0.19	3.28	2.10	2.09	7.18	7.00	6.96	10.40	9.96E+07	0.21
Averages σ(%)				7.22			10316.27			22.64		0.20
Absolute Average Error			0.05			0.39			1.64		2.67E+06	

As with using ^{137}Cs as a source, ^{238}U also required a lower level discriminator be applied before analyzing the input unknown spectra. This cut off level was placed at the 32^{nd} channel at approximately 195 keV and chosen because of its ability to remove the largest low energy feature. It should be noted that in some of the 30 trial runs of the initial input spectra, the tri-linear model did not always generate answers that could be resolved. This aspect of the solution was attributed to the noise produced by the testing algorithm to simulate a realistic spectrum and thusly if the spectra had larger counts collected the signal to noise ratio would be reduced and solutions could be found. An interesting feature of the tri-linear interpolation was that the solution to the problem was not always correct in its evaluations. The thicknesses of the materials might have been incorrect but the overall fit was successful and could easily be seen in the reduced χ^2 to the input spectrum. Also, despite the correctness of the thicknesses of the materials, the linear fitting parameter was proven to be accurate and therefore the source strength could be properly accessed. Given no initial information about the input spectrum, these fits to the problem then become a viable solution to the shielding thickness despite their incorrectness.

Chapter 7

Fully Automated Shielding Thickness Determination

The tri-linear model used in the MCLLS method demonstrated that it could generate reasonable solutions for determining the thicknesses of lead, aluminum and wood given the correct initial guesses. This ability is the foundation of the work proposed here but in order for this to be put to practical use, initial guesses for the non-linear parameters must be automatically made. The automated aspect of the initial guess making process is essential because it allows a wider variety of end users to operate a final product that could use this technique.

The algorithm developed to solve this problem, where a large amount of information is unknown about a spectrum, considered many different initial solutions to the final answer when given only an input to be analyzed. This approach assumed that the input spectrum had its background removed and that the direct transmissions from the radioisotopes along with interactions from the surrounding material were present. The program developed to execute the algorithm first started by performing a linear stripping

technique. It began by finding the peak locations of spectra used when calibrating the detector to convert from channel number to energy bin. These calibration spectra were created using the same source location that the previous libraries used but in this case all of the shielding material was removed. The sources used in this development were ^{22}Na, ^{60}Co, ^{137}Cs, ^{133}Ba and ^{238}U but in reality, any combination of sources and their associated peaks could be used.

Finding each of the peaks within each individual spectrum made use of the second derivatives based on the Gaussian distribution. The 1D second derivatives of a Gaussian were determined over a range of ±five channels from the point in consideration and the standard deviation of the fit had been chosen as 1E8 which was regarded as significantly large. The basic equations used were as follows:

$$g(x) = e^{-\frac{x^2}{2\sigma^2}} \tag{7.1}$$

$$g'(x) = -\frac{1}{2\sigma^2} 2x e^{-\frac{x^2}{2\sigma^2}} = -\frac{x}{\sigma^2} e^{-\frac{x^2}{2\sigma^2}} \tag{7.2}$$

$$g''(x) = (\frac{x^2}{\sigma^4} - \frac{1}{2\sigma^2}) e^{-\frac{x^2}{\sigma^2}} \tag{7.3}$$

This type of differentiation was chosen because if the standard deviation was reduced and the range of channels about the center point was altered, then the differentiation acts similar to a smoothing algorithm. Both of these parameters could be adjusted as needed to either increase or decrease the amount of smoothing used before further calculations were performed.

After the derivatives have been calculated along the entire spectrum, the peaks were then searched for. This was done by using the locations where these derivatives experience a local minimum. The location was found by locating a single channel where the average

of the five derivatives to the left of the point in question was negative and the average of the five derivatives to the right of the point in question was positive. This gives several possibilities of peak locations that can be attributed to the statistical noise within the spectra and the averaging of the derivatives. As a means to pick the most appropriate location, the derivative with the lowest value was chosen as a rough estimate of the peak location over a similarly grouped local minimum location.

This initial location was then selected and the process of fitting a Gaussian defined peak to the initial calibration spectrum at that location began. The technique used for choosing the range for the Gaussian fit was the opposite approach to finding the peaks where a local maximum is found on either side of the peak. This included finding the first location where the average of the five derivatives to the left of the location in question was positive and the average of the five derivatives to the right of the location was negative. This process was repeated as the first found location above and below the peak which acted as the range for the Gaussian fitting process. The Gaussian fitting process to the spectrum about the range found used the Numerical Recipes MRQMIN subroutine where a linear background was employed in order to reduce the need for human interaction on peak location and unknown obstructing convolutions with other peaks. After the fit had completed its calculation, the statistics of the fit were investigated. If the solution produced a result where the definition of the FWHM of the peak was equal to 0, then it was rejected. Also, the relative error to the initial input peak location was considered and if this was less than 1000.0 then it continues on and a peak was considered found. The amount of acceptable error may seem a bit more skewed than one would think but this was because the input to the system that generated the Gaussian fit was being provided MCNP5 post-processed spread data which was given in relative intensity. These input spectra values were on the order of 10E-6 which could contribute to the tolerance in the

error. As before, the value of the cutoff could be adjusted to fit any given situation.

All of the processes were repeated for every unshielded calibration file and for every found peak within each spectrum but this did not guarantee finding all of the peaks. This was because the end goal was to produce a table of centroid peaks and their associated FWHM with a high degree of confidence in their values to make comparisons with when the input unknown spectrum is treated. These judgments were made by creating a second order power series fit of the centroid to their associated FWHM.

$$y(x) = e^{C} x^{Aln(x)+B} \tag{7.4}$$

Where A, B, and C were the found empirical constants as 0.8951, -2.053 and -0.0417 respectively. This type of equation was chosen to better fit the known non-linearity that NaI(Tl) detectors experience between the deposited energy of the incident particle and the response recorded. Figure 7.1 demonstrates the relationship that was automatically generated between the found peaks and their associated FWHM though using the second order power series fit.

Now that an equation had been created, the input unknown spectrum peak values were searched for and their corresponding FWHM were found in the same fashion as the calibration spectra. Again, as with the calibration spectra, the cutoff could be adjusted to find the most accurate locations but for this application, it had been determined as 1000.0. In this instance, when the peaks for the input spectrum were found and characterized, they were compared to the centroid values and the FWHM of the unshielded calibration spectra. After identifying the peak, if the difference in the FWHM of the found centroid to the fitted second order power series equation was greater than 0.05, then the peak was

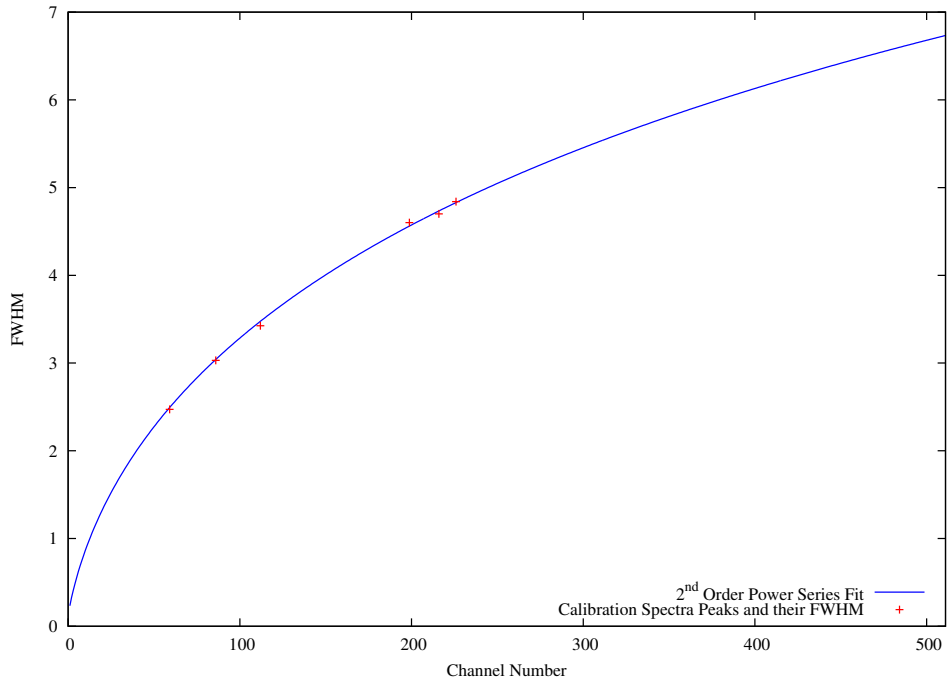

Figure 7.1: Peaks VS FWHM and the $2^n d$ Order Power Series Fit

considered convolved and is then skipped. This was done to choose the correct library to later decide the shielding material thicknesses and to determine if there was a shielded library for the peaks found within the spectrum. Next, this portion of the program then strips out the un-attenuated library from the input spectrum from using a ratio of the heights of the centroid values in both spectrums. It then returns the value that the library was multiplied by along with an updated spectrum where zeros have been entered above the highest channel in the library to reduce later confusion with finding a solution.

Taking into consideration that the highest peak of an unshielded spectrum was fit to a corresponding spectrum that was shielded of the same radioisotope, the result will produce obvious positive residuals below its identifying peak. This was the basis of an automatic decision made by the program to determine if it can continue to solve the problem and produce a solution to the thickness of the shielding materials. Given the

situation that the residuals were statistically defined as noise, the program stops but if the program finds that the residuals have a distinctive shape and the linearly stripped radioisotope had a corresponding shielded library, the program moves onto a non-linear search of the shielding materials.

The search for the shielding materials began by attempting to choose estimates for each of the eight sectors created by the 27 libraries. These sectors formed from the three thicknesses of the three shielding materials. Determinations of the initial estimates for the thicknesses began by fitting the peak heights of all 27 spectra within the library to the found peak centroid within the unknown spectrum. The scaling multipliers for each spectrum were recorded. Then, analysis of an upper limit to the channels was automatically calculated. As with the testing phase of the previous chapter, this calculation began by determining what the FWHM of the identifying centroid value was by using the second order power series fit that was previously created. The limit was then set as twice the distance of the calculated FWHM below the corresponding centroid value. This location was selected as a means to help disassociate the high degree of correlation that all 27 spectra have about the peak and to focus more on the interactions of the gamma particles which were more indicative of the shielding materials. The residuals of the peak fit solution from channel 0 to the upper limit were then averaged for each of the 27 libraries and the results were recorded. Also, as a means to help predetermine the appropriate thicknesses, the program CEARLLS (another CURMOD application) was automatically executed for an input of the unknown spectrum and each of the 27 libraries peak fits from channel 0 to the upper limit. CEARLLS performs a full spectrum linear fit for each of the libraries about the entire range permitted to the input unknown spectrum and produced results for: the scaling factor, the percent of the standard deviation, R, the percent of the area that was covered, the χ^2 of the fit and the average of the residuals.

These partial solutions were able to produce an initial rough estimate of the sector that the input spectrum resides in which helps to define the range of each of the materials thickness.

Now that each of the spectra within the library had an associated value of how well it fits the input spectrum, an interpolation was made within each of the eight sectors. This was done by using tri-linear interpolation where the limits of the bounds were determined by the thicknesses of the materials that define each sector. The point of interpolation was determined by producing a fraction in each direction that corresponds to the material based off of the absolute value of the average of the residuals from the peak fit. This fraction was the sum of the four lower defining bound averages over the sum of all eight edges of the sector. Each material fraction in each sector was comprised of the same eight values but the arrangement of the lower bounds for each material was different. Once the fractions have been determined, the tri-linear interpolation occurs at each channel and a new spectrum was produced. This entire process was repeated for each of the eight sectors. As with the 27 library spectra, results were produced when each of the eight sectorss interpolated spectra were fit at the peak centroid and also through application of CEARLLS from channel 0 to the channel defined by the upper limit.

After some preliminary calculations had been completed for each sector, the process of choosing the correct sector became an automated decision process. The major idea on how to make these decisions was to consider a number of tests so that the correct scenario will score the highest grade and therefore become the most likely candidate for a solution. When given a situation where the spatial location was sufficiently close to a sector boundary, several test cases would be necessary to confidently determine the true solution because the incorrect sector could inadvertently be chosen. These test cases and their associated choices were also weighted differently depending on the accuracy of the

answer.

The first test case chooses the sector that had the lowest average residual value from the peak fitting process and its sister test chose the sector that has the lowest average residual value from the CEARLLS program. These two tests were weighted equally. The next test series that was weighted slightly less than the previous tests used the statistical outputs generated from CEARLLS. These tests chose the sector that had the smallest value for the percent of standard deviation and the χ^2 that was closest to a value of one. Also, these tests chose the sector with the highest value for R and the percent of the area under the curve that was successfully fit.

After making these initial choices, the next step was to consider the residuals created when the eight sectors interpolated spectra were subtracted from the input unknown spectrum when the interpolated spectra were fit to the defining peak. A linear fit was then created upon each of the residuals and the statistical values of the total sum of squares and the residual sum of squares are determined. The idea was that the sector that had the best fit will have the lowest slope, y-intercept and both statistical values. Each sector that had the lowest of each of these parameters receives a winning choice value where the slope and y-intercept are weighted slightly less than the statistical successes. If the sector receives a value for the absolute value of the y-intercept of the linear fit to the residuals that was larger than is the identifying peak centroid height raised to the 2/3, the sector was then rejected for later analysis. This was done as a means to help remove sectors that had no relevance to solving the problem of the unknown thicknesses of shielding materials.

The last analysis performed before determination of the most correct sector and subsequent thickness, involved the tri-linear interpolation model of the MCLLS technique where three materials act as the three coordinates and each direction was the corre-

sponding thickness. The non-linear parameters require an initial guess for the search to be successful which were recycled from the previous solution that generated the general interpolated spectra for each sector. Each sector that passed the previous situation where the y-intercept was within an acceptable range was analyzed by this MCLLS technique. The input spectrum for the sectors to be inspected were slightly adjusted by using the original input unknown spectrum that was subtracted by the found residuals using the peak fit interpolated spectra from each sector. This was done as a means to help reduce unwanted features that could reside within the Compton continuum from a poor background removal and can be turned on or off depending on the application desired. Once the subtraction had been made, the adjusted input spectrum would be superficially smooth, so statistically distributed noise was then added to the signal to improve the statistical output. The output of this fit produces the found values for each of the four parameters (lead, aluminum, wood and linear scaling), their associated standard deviation and the χ^2 of the fit. Of the remaining sectors available for selection, the sector with the lowest total percent of standard deviation was allowed to make a choice on the appropriate sector as well as the sector that produce a χ^2 that was closest to one.

The final choice of the sector that was most suitable for the input unknown spectrum was the location with the most number of choices made. This then produced the answers for the thicknesses of the three unknown materials and concludes this approach. The technique developed requires no user interaction or knowledge of the energy distribution that any particular radionuclide produces and how the shielding material will alter the distribution collected. The only task that the user would be required to perform would be to ensure that the input spectrum had the same calibration as the libraries because without this alignment, the entire process is useless.

Chapter 8

Testing the Automation Procedure

A procedure now had been proposed and it must be tested to ensure its ability to resolve the input unknown spectrum. As with before, only one test case scenario will be fully disclosed and all other solutions will only have the final conclusion presented. The test case used will use ^{137}Cs as a source with the first data set libraries, which uses the spectrum produced from using the Unknown 1 shielding material configurations in table 5.1. As with the previous test, the input spectrum was multiplied by 10^8 and statistical noise was added before being analyzed by the program.

Given that no other sources were present within the input spectrum, the algorithm quickly recognized that the single energy photo peak of ^{137}Cs though implementation of the spectrum stripping approach which can be seen in the figure 8.1. The residuals from the linear stripping technique demonstrated that there was shielding material present in the collected spectrum. The linear value used to fit the yield of the unshielded calibration ^{137}Cs spectrum was 4.43E7 which was sufficiently below the correct value.

Next, the algorithm finds correlations of the input spectrum to all of 27 library spectra though both a peak fit approach and though a full spectrum linear fitting routine. The

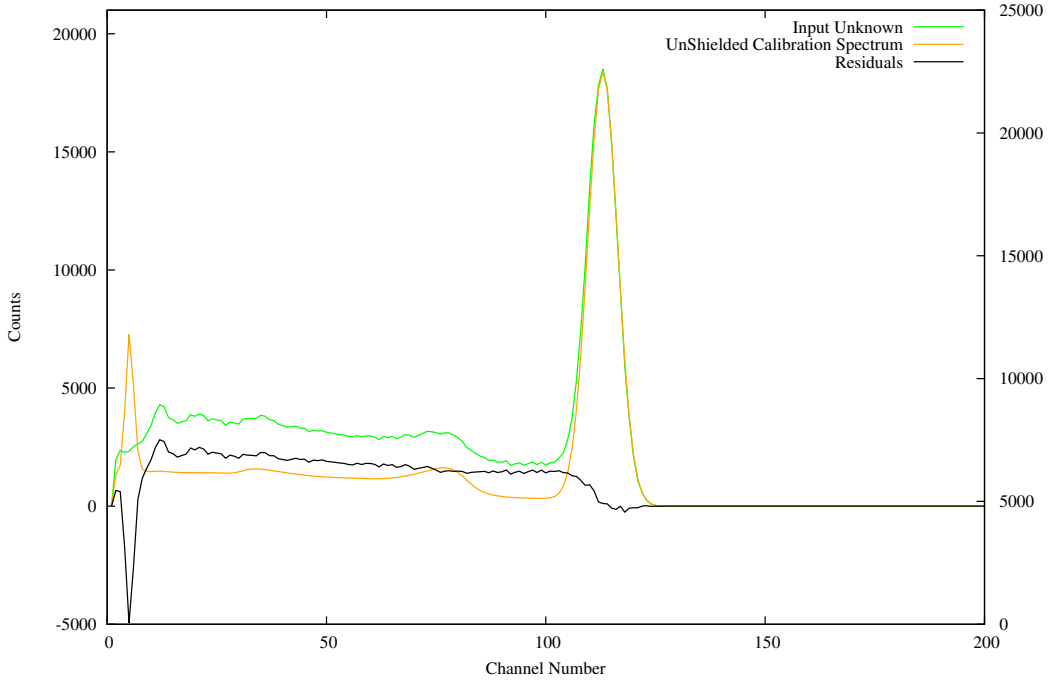

Figure 8.1: Linear Stripping and Shielding Material Presence Determination

upper limit of the calculations used beyond the peak fitting approaches was found to be located at the 103^{rd} channel as was also previously determined. The results of the two preliminary correlation approaches were as follows in table 8.1:

These correlations showed that the backgrounds for both the peak fitting and CEARLLS routines were generally lower when the configurations of m and s were present in the correlations and that all of the fits using the CEARLLS approach resulted in very poor χ^2 values.

Out of these known incorrect initial values, fractions were generated to create the interpolated spectrum from the libraries for each sector. The correct sector for this example produced fractions that where 0.489, 0.437 and 0.528 for lead, aluminum and wood respectively. Similar initial fractions were created for each of the eight sectors and out of these assessments; the initial guesses were made for each sector. Table 16 holds these

Table 8.1: Preliminary Correlations to the Unknown Input Spectrum

	Peak Fitting		CEARLLS			
Library	Avg Bkg	SigmaA(%)	R	AREA(%)	ChiSq	Avg Bkg
mmm	598.418	0.181	0.809	65.379	318.053	10.719
mmp	-189.142	0.181	0.809	65.477	317.149	6.332
mms	247.709	0.18	0.81	65.53	316.661	3.957
mpm	-674.103	0.181	0.808	65.335	318.457	12.684
mpp	-1760.524	0.182	0.803	64.5	326.13	49.951
mps	-1195.161	0.181	0.807	65.051	321.064	25.343
msm	-5.16	0.18	0.81	65.569	316.306	2.237
msp	-919.879	0.181	0.807	65.145	320.205	21.172
mss	-454.307	0.181	0.809	65.481	317.115	6.165
pmm	375.371	0.181	0.807	65.078	320.818	24.152
pmp	-448.117	0.18	0.809	65.518	316.777	4.523
pms	-27.905	0.181	0.809	65.388	317.973	10.33
ppm	-954.303	0.181	0.809	65.383	318.01	10.513
ppp	-1928.643	0.181	0.805	64.822	323.169	35.57
pps	-1440.979	0.181	0.807	65.205	319.654	18.495
psm	-247.29	0.181	0.809	65.4	317.86	9.781
psp	-1120.312	0.181	0.808	65.324	318.553	13.15
pss	-682.919	0.181	0.809	65.486	317.066	5.924
smm	486.631	0.181	0.808	65.238	319.347	17.006
smp	-321.087	0.18	0.809	65.527	316.695	4.126
sms	106.195	0.181	0.809	65.497	316.968	5.449
spm	-793.168	0.181	0.809	65.425	317.625	8.644
spp	-1865.538	0.182	0.804	64.654	324.709	43.052
sps	-1319.363	0.181	0.808	65.206	319.637	18.415
ssm	-114.316	0.18	0.809	65.529	316.676	4.032
ssp	-1065.462	0.181	0.808	65.292	318.848	14.584
sss	-544.532	0.18	0.81	65.544	316.533	3.337

Table 8.2: Initial Guesses for Each Sector

Sector	Lead	Aluminum	Wood
1	0.267	1.640	5.466
2	0.274	2.025	9.468
3	0.277	2.532	6.037
4	0.273	2.655	8.526
5	0.445	1.580	5.267
6	0.443	1.380	8.277
7	0.440	2.579	4.811
8	0.445	2.672	8.580

guesses in centimeters that were used if the spectra they produced passed several of the preliminary tests.

As with all 27 library spectra, correlations were found for each of the eight interpolated spectra using both the peak fit and CEARLLS approaches. The correlations from the interpolated spectra based off of the initial guesses allowed for choices to be made on the correct sector. Sector 5 scored for the lowest average background when the peaks were matched, sector 1 scored the lowest $\%\sigma$ and highest R along with the lowest χ^2 and average background from CEARLLS.

Residuals were then created from the output of CEARLLS and a linear trend was fit to the results from each sector. These then show some interesting trends which become more prevalent when the statistical tests of the total sum of squares and the residual sum of squares. Table 8.4 shows these results where the values of m and b correspond to the standard slope intercept equation.

Based off of these results, sectors 3, 4 and 8 were omitted from further contribution to the selection of the correct sector because their slope and y-intercept values were above

Table 8.3: Correlations from Each Interpolated Sector

Library	Peak Fitting Avg Bkg	SigmaA(%)	CEARLLS R	AREA(%)	ChiSq	Avg Bkg
1	10.628	0.162	0.903	65.501	170.387	5.279
2	-127.761	0.162	0.902	66.032	170.635	-18.416
3	-737.981	0.163	0.899	67.396	176.158	-79.276
4	-1335.657	0.164	0.893	67.871	186.419	-100.470
5	4.280	0.162	0.902	65.305	171.355	14.021
6	-231.252	0.162	0.902	66.299	171.132	-30.343
7	-511.551	0.162	0.901	66.958	172.898	-59.727
8	-1071.129	0.163	0.897	67.839	179.733	-99.045

Table 8.4: Slope, Y-Intercept and Sum of Squares Statistics for Each Sector

Sector	m	b	SSerr	SStot
1	-0.806	53.323	349738	412334
2	1.606	-212.858	619954	868622
3	6.332	-1073.562	7750770	11617900
4	14.849	-2122.680	24957900	46228100
5	-3.162	171.889	733356	1698050
6	-0.219	-219.642	672791	677420
7	1.240	-577.253	2090820	2239050
8	8.457	-1519.376	12034400	18934100

Table 8.5: Final Choices before Sector Selection

Sector	χ^2	Total $\%\sigma$
1	1.084	0.136
2	1.042	0.174
5	1.310	0.150
6	0.919	0.175
7	1.096	0.123

Table 8.6: Final Answer

	A [cm]	SigmaA	$\%\sigma A$
Pb	0.264	0.003	1.24
Al	2.000	0.079	3.96
Wood	4.482	0.369	8.22
Linear	1.06E+08	1.92E+05	0.18

the thresholds. Of the remaining sectors, sector 6 had the lowest slope, but sector 1 had the lowest y-intercept, residual sum of squares and total sum of squares. The remaining sectors of 1, 2, 5, 6, and 7 were then allowed to proceed onto the non-linear search portion of the final material thickness selection.

The final choices made before all of the tallies for each sector were summed and a decision was made selected sector 2 for the closest χ^2 value to 1 and sector 7 as the location with the lowest summed $\%\sigma$ for the thicknesses of the materials. The final selection of the entire process chose sector 1 with 62% of all the available votes that could have been spread out over all eight sectors. This was the correct decision. The final solutions to the problem that was automatically generated can be found in table 8.6.

The answers produced were deemed as acceptable solutions to the problem submitted

to the automatic non-linear parameter guessing algorithm. As with the previous testing package, the same input spectra whose material thicknesses were unknown to the algorithm were used. 48 total spectra were used and the program was allowed to make the initial guesses for the non-linear parameters and make the final decision on the sector that it found to be the most appropriate solution to the input problem. The results for the first data set ranging from the mmm to ppp configurations can be seen in table 8.7.

Table 8.7: First Data Set Library Using ^{137}Cs with Automatic Guesses Generated

	χ^2	Pb TRUE	Pb Meas.	Pb σ(%)	Al TRUE	Al Meas.	Al σ(%)	Wood TRUE	Wood Meas.	Wood σ(%)	Amount Meas.	Amount σ(%)	Win %
unk1	1.084	0.20	0.26	1.24	1.96	2.00	3.96	5.00	4.48	8.22	1.06E+08	0.18	61.90
unk2	0.989	0.30	0.26	1.89	2.00	1.93	5.98	8.50	8.92	4.89	9.51E+07	0.19	71.43
unk3	1.119	0.25	0.25	1.54	3.20	3.01	2.62	4.00	4.55	8.66	9.72E+07	0.19	52.38
unk4	0.935	0.19	0.27	2.09	2.80	2.84	3.88	10.00	9.06	4.95	1.07E+08	0.18	78.26
unk5	1.076	0.51	0.44	1.01	2.10	2.11	5.01	6.00	5.62	8.40	8.98E+07	0.21	38.10
unk6	0.895	0.50	0.44	1.34	1.46	1.78	7.58	9.04	8.24	6.09	9.51E+07	0.21	66.67
unk7	1.279	0.40	0.45	1.15	2.60	2.51	4.04	4.50	5.43	8.55	1.06E+08	0.20	42.86
unk8	1.044	0.52	0.46	0.41	3.10	3.16	1.22	9.40	9.15	1.76	9.99E+07	0.17	100.00
Averages σ(%)				1.33			4.29			6.44		0.19	
Abs Avg Error			5.25E-02			1.02E-01			5.99E-01		5.24E+06		

It should be noted that despite the winning percentage of votes cast for the unknown spectra 5 and7 being below %50, the correct sector was chosen. This winning percentage was spread through all of the eight sectors and in these cases the distribution was more spread out than with the other cases and the correct sector still received the largest percentage of the scores. Also, the linear parameter for the amount of the radioisotope present was well within an acceptable range to make accurate assessments of the strength of the source.

Table 8.8: First Data Set Library Using ^{60}Co with Automatic Guesses Generated

	χ^2	Pb TRUE	Pb Meas.	Pb σ(%)	Al TRUE	Al Meas.	Al σ(%)	Wood TRUE	Wood Meas.	Wood σ(%)	Amount Meas.	Amount σ(%)	Win %
unk1	1.058	0.20	0.27	2.87	1.96	1.85	6.02	5.00	4.95	10.46	1.02E+08	0.15	71.43
unk2	1.095	0.30	0.26	4.09	2.00	1.85	7.74	8.50	9.11	6.60	9.69E+07	0.15	57.14
unk3	1.106	0.25	0.25	2.66	3.20	2.91	3.06	4.00	5.46	7.69	9.91E+07	0.15	71.43
unk4	1.013	0.19	0.27	3.52	2.80	2.93	4.11	10.00	9.06	5.76	1.05E+08	0.15	78.26
unk5	1.161	0.51	0.43	1.65	2.10	2.08	5.31	6.00	5.69	9.13	9.37E+07	0.16	42.86
unk6	1.064	0.50	0.45	2.81	1.46	1.53	11.80	9.04	9.28	7.48	9.73E+07	0.16	71.43
unk7	1.113	0.40	0.46	1.50	2.60	2.36	3.91	4.50	6.08	6.51	1.03E+08	0.15	57.14
unk8	0.948	0.52	0.45	2.09	3.10	3.19	3.99	9.40	9.16	6.18	9.62E+07	0.16	100.00
Averages σ(%)				2.65			5.74			7.48		0.15	
Abs Avg Error			5.63E-02			1.38E-01			6.79E-01		3.35E+06		

Table 8.9: First Data Set Library Using ^{238}U with Automatic Guesses Generated

	χ^2	Pb TRUE	Pb Meas.	Pb σ(%)	Al TRUE	Al Meas.	Al σ(%)	Wood TRUE	Wood Meas.	Wood σ(%)	Amount Meas.	Amount σ(%)	Win %
unk1	1.067	0.20	0.24	1.76	1.96	2.00	6.10	5.00	5.76	10.42	1.05E+08	0.18	85.71
unk2	1.171	0.30	0.27	2.12	2.00	1.61	9.11	8.50	10.21	6.03	9.31E+07	0.20	47.62
unk3	1.174	0.25	0.28	1.72	3.20	2.91	4.33	4.00	5.63	10.86	9.93E+07	0.20	71.43
unk4	1.357	0.19	0.25	2.45	2.80	2.56	5.77	10.00	9.03	7.00	9.39E+07	0.20	100.00
unk5	1.32	0.51	0.44	1.20	2.10	2.12	6.63	6.00	5.16	13.52	9.14E+07	0.22	52.38
unk6	1.064	0.50	0.46	1.16	1.46	1.90	6.92	9.04	7.56	8.05	9.74E+07	0.22	61.90
unk7	1.108	0.40	0.45	1.18	2.60	2.73	4.56	4.50	4.99	11.54	1.07E+08	0.21	80.95
unk8	1.092	0.52	0.43	1.85	3.10	2.92	5.75	9.40	9.75	7.42	8.78E+07	0.23	82.61
Averages σ(%)				1.68			6.15			9.36		0.21	
Abs Avg Error			5.13E-02			2.16E-01			1.03E+00		6.14E+06		

In general, the first data set demonstrated that each of the algorithms was successful in locating the correct sector and producing sufficiently accurate solutions for the thicknesses of the materials. The results for the first data set ranging from the null to sss configurations can be seen in table 8.10.

Table 8.10: Second Data Set Library Using ^{137}Cs with Automatic Guesses Generated

	χ^2	Pb TRUE	Pb Meas.	Pb σ(%)	Al TRUE	Al Meas.	Al σ(%)	Wood TRUE	Wood Meas.	Wood σ(%)	Amount Meas.	Amount σ(%)	Win %
unk1	0.800	0.10	0.26	1.29	1.00	0.37	17.21	2.00	4.92	4.27	1.16E+08	0.18	52.38
unk2	0.816	0.05	0.10	3.07	0.50	0.69	9.68	6.80	5.21	6.55	1.05E+08	0.18	66.67
unk3	1.163	0.15	0.27	1.20	1.50	1.35	3.09	1.00	1.93	11.22	1.14E+08	0.19	42.86
unk4	1.206	0.08	0.27	1.67	1.80	1.41	6.44	4.80	5.73	6.85	1.19E+08	0.18	69.57
unk5	0.804	0.20	0.26	1.35	0.70	0.39	17.21	3.30	5.01	4.39	1.05E+08	0.19	42.86
unk6	0.752	0.30	0.27	1.27	0.30	0.57	12.39	6.00	5.33	4.22	9.76E+07	0.20	71.43
unk7	1.084	0.25	0.28	1.14	1.70	1.73	2.61	2.50	2.29	10.63	1.02E+08	0.20	76.19
unk8	1.065	0.19	0.27	1.22	2.10	2.16	4.27	7.00	5.35	7.80	1.04E+08	0.19	91.30
Averages σ(%)				1.53			9.11			6.996		0.19	
Abs Avg Error			9.00E-02			2.54E-01			1.33E+00		8.43E+06		

As with the test cases, a lower level discriminator was placed on the input spectrum and library spectra at 12^{th} channel. In these test scenarios, the correct sector was not always chosen. These inconsistent solutions stem from a vast array possibilities ranging from incorrect initial guesses for the non-linear parameters and from inaccuracies in the creation of the libraries used. In particular the input of Unknown1 chose sector 6, Unknown 3 chose sector 7, Unknown 4 chose sector 8 and Unknown 5 chose sector 6. In some cases this caused more problems in the inaccuracy of the solution as in the Unknown 1 where the thickness of wood was drastically off. With the other cases, the values used were not radically different and the ultimate values used were not even within the starting sector of the parameter guesses created. This facet of the program indirectly demonstrates some flexibility of the tri-linear model to adapt its solutions to better fit the input spectra. No lower boundary was placed on the solutions produced for ^{60}Co. The solutions found using this source were found to be successful and over sufficiently accurate. The inputs that used ^{238}U also used a lower level discriminator at the 32^{nd} channel. These scenarios also produced incorrect sector selection but ultimately generated sufficient final solutions for the thicknesses of the shielding materials.

Table 8.11: Second Data Set Library Using ^{60}Co with Automatic Guesses Generated

	χ^2	Pb TRUE	Pb Meas.	Pb σ(%)	Al TRUE	Al Meas.	Al σ(%)	Wood TRUE	Wood Meas.	Wood σ(%)	Amount Meas.	Amount σ(%)	Win %
unk1	1.094	0.10	0.11	2.96	1.00	0.86	8.80	2.00	2.17	18.47	9.85E+07	0.14	52.38
unk2	1.083	0.05	0.10	5.84	0.50	0.62	22.28	6.80	5.53	12.24	1.02E+08	0.14	66.67
unk3	1.807	0.15	0.18	2.37	1.50	1.42	3.07	1.00	1.61	12.78	1.01E+08	0.14	71.43
unk4	1.138	0.08	0.27	2.60	1.80	1.42	6.65	4.80	5.73	7.13	1.09E+08	0.14	61.90
unk5	1.662	0.20	0.22	2.30	0.70	0.67	8.79	3.30	3.41	7.16	1.00E+08	0.14	57.14
unk6	1.075	0.30	0.26	2.97	0.30	0.46	21.25	6.00	5.42	6.73	9.81E+07	0.15	71.43
unk7	1.101	0.25	0.27	1.56	1.70	1.78	2.60	2.50	2.04	11.18	1.01E+08	0.15	76.19
unk8	1.833	0.19	0.22	3.31	2.10	2.18	4.58	7.00	6.68	7.11	1.01E+08	0.15	100.00
Averages σ(%)				2.99			9.75			10.35		0.14	
Abs Avg Error			4.88E-02			1.34E-01			5.56E-01		2.18E+06		

Table 8.12: Second Data Set Library Using ^{238}U with Automatic Guesses Generated

	χ^2	Pb TRUE	Pb Meas.	Pb σ(%)	Al TRUE	Al Meas.	Al σ(%)	Wood TRUE	Wood Meas.	Wood σ(%)	Amount Meas.	Amount σ(%)	Win %
unk1	1.94	0.10	0.16	0.74	1.00	1.25	3.62	2.00	3.59	6.79	1.11E+08	0.18	85.71
unk2	1.895	0.05	0.10	6.17	0.50	1.35	25.26	6.80	5.39	34.16	1.12E+08	0.18	66.67
unk3	1.645	0.15	0.18	4.42	1.50	2.02	8.58	1.00	1.32	59.47	1.10E+08	0.19	42.86
unk4	1.916	0.08	0.11	5.35	1.80	1.87	18.68	4.80	3.77	52.38	1.01E+08	0.19	57.14
unk5	1.624	0.20	0.25	2.95	0.70	1.64	10.58	3.30	1.67	44.28	1.12E+08	0.20	33.33
unk6	1.34	0.30	0.33	0.83	0.30	0.92	13.31	6.00	4.21	15.49	1.05E+08	0.21	38.10
unk7	1.458	0.25	0.26	2.99	1.70	1.6	11.60	2.50	2.62	29.25	9.94E+07	0.21	39.13
unk8	0.922	0.19	0.24	3.25	2.10	1.79	12.44	7.00	6.34	16.12	9.36E+07	0.22	42.86
Averages σ(%)				3.34			13.01			32.24		0.20	
Abs Avg Error			3.88E-02			4.58E-01			1.07E+00		7.25E+06		

Chapter 9

Conclusions

The tri-linear model approach used in a MCLLS application for material thickness identification that used a vast array of forward calculations was successful. All of the answers generated using this technique would not have created any solution to the problem presented if the forward library calculations had not been thoroughly and accurately modeled. These libraries are also one of the most limiting factors of this approach because if a library has not yet been constructed, the algorithm is ultimately unable to produce a solution however wrong it may be.

The algorithm demonstrated its ability to adapt and change the boundaries used in its interpolation process to better fit the input spectra despite the inaccuracy of the initial guesses for the non-linear parameters. This is important because it allows a wider range of techniques to find initial guesses for a final accurate solution. It also has demonstrated that if there are inconsistencies in shape and magnitude of the libraries created, the algorithm has difficulty in resolving a proper solution. As a means to address this, lower level discriminators can be added to reduce confusion within the solving routine. Also, the tri-linear interpolation approach proved as a successful method for determining the

overall source strength. Regardless of the correct values chosen given any of the various input unknown spectra, the linear parameter proved itself to be sufficiently accurate. This is very useful because the strength of the source can be used to determine if the amount found could be harmful to the public at large or if it is relatively benign.

The testing situations presented do not completely demonstrate the strength of the technique but rather an extraneous case that would be less than ideal for a realistic scenario. The answers calculated, vary in the percentage chosen to the other sectors based on the radionuclide used and the overall magnitude and statistical fluctuations of the input spectrum. As it currently stands, the correct sector was always chosen if the input spectrum had at least 1000 counts at the peak location when the background was subtracted out and the proper initial guesses for the non-linear parameters were provided. In some instances, the correct sector was chosen when the peak counts were substantially less but this is a case by case scenario and cannot be fully trusted. Overall, as the counts become higher, the statistical fluctuations decrease and the accuracy of the correct sector chosen increases.

In a practical application, this method could prove itself to be successful in determining the approximate shielding thicknesses of a source but more importantly it would be able to determine the overall strength of the source. This is very important given a condition where the container could be holding a malicious radioisotope and the appropriate staff would need to know as much information about the container before fully addressing the situation. The library creation process would also be of extreme importance because without the most likely situation modeled for its specific application, the resulting parameter values could be drastically incorrect.

Chapter 10

Future work

To further complete this technique, the automatic process of removing slight changes in the background would be included along with the incorporation of the gain shifting program GSHIFT. This would help the user to adjust the input spectrum to be aligned with the libraries and ensure a correct answer. This entire technique would then be transformed into an internet browser based GUI. This would further help the end user to graphically see the produced results and to help maintain the control and distribution of the source code generated.

One aspect that the technique has set out to accomplish but yet has been completed was to deal with alterations within the collected background. The basic idea to carry out this task would be to require the user to supply a best guess as to the background which would then be subtracted from the input spectrum until a certain amount of acceptable negative values would be produced. This updated spectrum would then be input into the existing technique and solved the exact same way.

Also, there are a variety of methods to produce initial guesses for the non-linear parameters. One particular method would be to randomly choose locations for each of

the materials in each of the sectors. Once these guesses have been made, perform the non-linear search and compare the answers produced. The process would be repeated multiple times and a gradient search would then be applied to the found results to locate the correct values for each material.

Another possibility would be to further assist the tri-linear method in a more realistic manner of interpolation. This idea stems from the fact that photon radiation does not behave in a linear fashion as it is attenuated through materials but more of in an inverse exponential manner. One approach to assist in better interpolated values would be to adjust the fraction used at each energy bin based off of the mass attenuation values for each material about the guessed thickness. This would possibly increase the computation time due to the large amount of numerical interpolation for each mass attenuation value but its overall accuracy of the solution might improve.

Given that all of the spectra used in the library creation and in implementing input unknown spectra were created using MCNP, this process needs to be tested using actual real collected data. As a means to accomplish this, the exact same geometric conditions would be used. ^{137}Cs and ^{60}Co would be used as sources and sufficiently long enough run times would be allowed to ensure the validity of the spectra produced for the library creation. Several of the test unknown geometric configurations would also be created to demonstrate the techniques ability at finding a true solution.

In general, a wide variety of shielded scenarios should be considered to fully characterize this approach for determination of the thicknesses of shielding materials. This would include different types of materials, different geometric configurations of the shielding materials, more gamma particle emitting radio nuclides, detector geometric configurations, detector material composition and many more. Work will continue with MCLLS technique to find a wider range of possibilities and potential solutions for all types of

problems.

REFERENCES

Ahmad, M.S., Barrow, D.E., Little, E.A., and Szkopiak, Z.C. (1971). Computer Analysis of Complex Relaxation Spectra. J Phys D Appl Phys 4, 1460.

Allyson, J.D., and Sanderson, D.C.W. (2001). Spectral deconvolution and operational use of stripping ratios in airborne radiometrics. J Environ Radioactiv 53, 351-363.

Bevington, P.R., and Robinson, D.K. (2003). Data reduction and error analysis for the physical sciences, 3rd edn (Boston: McGraw-Hill).

Burr, T., Hamada, M.S., Graves, T.L., and Myers, S. (2009). Augmenting Real Data with Synthetic Data: An Application in Assessing Radio-Isotope Identification Algorithms. Qual Reliab Eng Int 25, 899-911.

Estep, R.J., and Sapp, B.A. (2008). Energy calibration algorithms for the multiple isotope material basis set (MIMBS) isotope identification method. 2008 Ieee Conference on Technologies for Homeland Security, Vols 1 and 2, 12-17.

Estep, R.J., Sapp, B.A., and Russ, W. (2007). Improved isotopic identification for NaI spectroscopic portal monitors using the material basis set (NOS) method. 2007 IEEE Conference on Technologies for Homeland Security: Enhancing Critical Infrastructure Dependability, 168-173.

Furr, A.K., Robinson, E.L., and Robins, C.H. (1968). A Spectrum Stripping Technique for Qualitative Activation Analysis Using Monoenergetic Gamma Spectra. Nucl Instrum Methods 63, 205.

Gardner, R.P., and Sood, A. (2004). A Monte Carlo simulation approach for generating NaI detector response functions (DRFs) that accounts for non-linearity and variable flat continua. Nucl Instrum Meth B 213, 87-99.

Gardner, R.P., Sood, A., Wang, Y.Y., Liu, L., Guo, P., and Gehrke, R.J. (1997). Single peak versus library least-squares analysis methods for the PGNAA analysis of vitrified waste. Appl Radiat Isotopes 48, 1331-1335.

Gardner, R.P., and Verghese, K. (1991). Monte-Carlo Nuclear Well Logging Benchmark Problems with Preliminary Intercomparison Results. Nucl Geophys 5,

429-438.

Gilmore, G. (2008). Practical gamma-ray spectrometry, 2nd edn (Chichester, England ; Hoboken, NJ: Wiley).

Guo, W.J., Gardner, R.P., and Todd, A.C. (2004). Using the Monte Carlo - Library Least-Squares (MCLLS) approach for the in vivo XRF measurement of lead in bone. Nucl Instrum Meth A 516, 586-593.

Heath, R.L. (1966). Computer Techniques for Analysis of Gamma-Ray Spectra Obtained with Nai and Lithium-Ion Drifted Germanium Detectors. Nucl Instrum Methods 43, 209.

Heath, R.L. (1998). Development of new expanded editions of the Gamma-ray Spectrum Catalogues in electronic format. J Radioanal Nucl Ch 233, 81-89.

Holmes, T.W., Calderon, A., Peeples, C.R., and Gardner, R.P. (2011). A proposed benchmark problem for cargo nuclear threat monitoring. Nucl Instrum Meth A 652, 52-57.

Jarman, K.D., Runkle, R.C., Anderson, K.K., and Pfund, D.M. (2008). A comparison of simple algorithms for gamma-ray spectrometers in radioactive source search applications. Appl Radiat Isotopes 66, 362-371.

Knoll, G.F. (2000). Radiation detection and measurement, 3rd edn (New York: Wiley).

Marchetti, A.A., and Mignerey, A.C. (1993). Deconvolution of Mass-Spectra. Nucl Instrum Meth A 324, 288-296.

Mattingly, J., and Mitchell, D.J. (2010). A Framework for the Solution of Inverse Radiation Transport Problems. Ieee T Nucl Sci 57, 3734-3743.

Mattingly, J., and Mitchell, D.J. (2012). Implementation and testing of a multivariate inverse radiation transport solver. Appl Radiat Isotopes 70, 1136-1140.

Meng, L.J., and Ramsden, D. (2000). An inter-comparison of three spectral-deconvolution algorithms for gamma-ray spectroscopy. Ieee T Nucl Sci 47, 1329-1336.

Metwally, W.A., Gardner, R.P., and Mayo, C.W. (2004). Elemental PGNAA

analysis using gamma-gamma coincidence counting with the library least-squares approach. Nucl Instrum Meth B 213, 394-399.

Mitchell, L.J., Phlips, B.F., Wulf, E.A., Hutcheson, A.L., and Leas, B.E. (2011). Cross Country Background Measurements with High Purity Germanium. 2011 Ieee Nuclear Science Symposium and Medical Imaging Conference (Nss/Mic), 319-323.

Mukhopadhyay, S., Guss, P., and Maurer, R. (2011). Current Trends in Gamma Radiation Detection for Radiological Emergency Response. Penetrating Radiation Systems and Applications Xii 8144.

Nelson, K.E., Gosnell, T.B., and Knapp, D.A. (2011). The effect of energy resolution on the extraction of information content from gamma-ray spectra. Nucl Instrum Meth A 659, 207-214.

Peel, J.B., and Willett, G.D. (1975). Photoelectron-Spectrum of Methylenimine by Spectrum Stripping. J Chem Soc Farad T 2 71, 1799-1804.

Press, W.H. (1996). FORTRAN numerical recipes, 2nd edn (Cambridge England ; New York: Cambridge University Press).

Salmon, L. (1961). Analysis of Gamma-Ray Scintillation Spectra by the Method of Least Squares. Nucl Instrum Methods 14, 193-199.

Sandness, G.A., Schweppe, J.E., Hensley, W.K., Borgardt, J.D., and Mitchell, A.L. (2009). Accurate Modeling of the Terrestrial Gamma-Ray Background for Homeland Security Applications. Ieee Nucl Sci Conf R, 126-133.

W. A. Wetwally, R.P.G., and Avneet Sood (2004). Gaussian Broadening of MCNP Pulse Height Spectra. Transactions of the American Nuclear Society 91, 2.

APPENDICES

Appendix A

sss Configuration MCNP Input Deck

```
sss Configuration
c        CELL CARD
    1     5   -3.67 11 -12 13 -14 15 -16  $             Detector
    2     8 -0.423419 (32 -22 23 -24 25 -26 ): $          Wood Box
            (21 -32 23 -24 25 -35 ):(21 -32 23 -24 36 -26 ):
            (21 -32 34 -24 -36 35 ):(21 -32 23 -33 -36 35 )
    3     2  -2.855272 (40 -41 44 -43 ):(41 -42 -43 ) $    Aluminum Cylinders
    4     1  -11.35796 (50 -51 54 -53 ):(51 -52 -53 ) $    Lead Cylinders
    5     1  -11.35 61 -62 63 -64 65 -66  $             Lead Base
    6     4    -2.7 17 -18 19 -20 10 -9 #1  $           Detector Can
    7     1  -11.35 67 -68 69 -73  $                    Lead Cylinder Under Det
    8     1  -11.35 70 -71 -69 72  $             Second Lead Cylinder Under Det
    9     8 -0.8336 -74 75 -76 77 -78 79  $              Woodend Table
 9998     9 -0.001205 -1 #1 #2 #3 #4 #5 #6 #7 #8 #9
 9999     0         1
```

```
c        SURFACE CARD
    1         s 50 0 0 100  $       Void Boundary
c        Detector
   11        pz 0  $        Bottom of Detect
   12        pz 40.64  $    Top of Detect
   13        py -5.08  $    Near Side of Detect
   14        py 5.08  $     Far Side of Detect
   15        px 100  $       Near Side of Detect
   16        px 105.08  $    Far Side of Detect
   17        pz -1.111
   18        pz 41.754
   19        py -5.556
   20        py 5.556
   10        px 99.682
    9        px 105.397
c        Wood Box (OUT-SIDE)
```

```
   21        pz 0  $        Bottom
   22        pz 35.0691667  $ Top
   23        py -21.1093  $  Near Side
   24        py 21.1093  $   Far Side
   25        px -21.1093  $  Near Side
   26        px 21.1093  $   Far Side
c        Wood Box (IN-SIDE)
   31        pz 0  $         Bottom
   32        pz 27.91978  $  Top
   33        py -13.95989  $ Near Side
   34        py 13.95989  $  Far Side
   35        px -13.95989  $ Near Side
   36        px 13.95989  $  Far Side
c        Aluminum Cylinder
   40        pz 0
   41        pz 10.53754  $   Lower Height of Cylinder
```

```
   42        pz 12.819106  $   Upper Height of Cylinder
   43        cz 7.819115  $    Outer Al Radius
   44        cz 5.53754  $    Inner Al Radius
c        Lead Cylinder
   50        pz 0
   51        pz 10  $        Lower Height of Cylinder
   52        pz 10.358364  $  Upper Height of Cylinder
   53        cz 5.358365  $   Outer Al Radius
   54        cz 5  $         Inner Al Radius
c         Lead Base
   61        pz -0.53754  $   Bottom
   62        pz 0  $         Top
   63        py -24.684  $  Near Side
   64        py 24.684  $   Far Side
   65        px -24.684  $  Near Side
   66        px 24.684  $   Far Side
```

```
c         Lead Cylinder Underneath the Detector
   67       c/z 102.54 0 2.54
   68       c/z 102.54 0 12.7
   69        pz -8.371
   73        pz -1.111
c         Second Lead Cylinder Underneath the Detector
   70       c/z 102.54 0 6
   71       c/z 102.54 0 8
   72        pz -23.371
c         Wooden Table
   74        pz -38
   75        pz -40
   76        py 24.684
   77        py -24.684
   78        px 115
   79        px 24.684
```

```
mode  p e
c
c       Material Card
m1    82206.               -1  $ Lead
m2    13027.               -1  $ Aluminum
m4    12000.            -0.01  $ Aluminum (6061-T6)
      13000.          -0.9715 14000.           -0.005 22000.           -0.001
      24000.           -0.002 25000.           -0.001 26000.           -0.005
      29000.          -0.0025 30000.           -0.002
m5    11000.         -0.15307  $ NaI(Tl) p=  3.67
      53000.          -0.8457
      81000.         -0.00123
m6    14000.               -1  $ Padding
m7    6000.04p              2  $ Reflector
      9000.04p              4
```

```
m8    6000.             -0.49  $ Wood
      1001.             -0.06 8016.             -0.44 7014.             -0.01
m9    1000.           -5e-007  $ Air
      2000.        -5.24e-006 6000.      -0.000104667 7000.          -0.78084
      8000.        -0.2096853 10000.      -1.818e-005 18000.         -0.00934
      36000.       -1.14e-006 54000.        -8.7e-008
c
c       Data Card
imp:p             1 1 1 1 1 1 1 1 1 1 0 $ 1, 9999
imp:e             1 1 1 1 1 1 1 1 1 1 0 $ 1, 9999
f8:p 1
e8 0.0 512i 3.0
sdef  par=2 pos=0 0 1  erg=D1
si1  L 0.00447  0.0318171 0.0321936 0.0364 0.66166
sp1  D 0.01  0.0196 0.036 0.0132 0.851
nps 750000000
```

Appendix B

^{238}U MCNP Source Definition

```
si1 S 2 3 $                      Two distributions for lines and groups
sp1 D  322741.1705  673363.3408 $ Both lines and groups are sampled
 #    si2       sp2 $              The photon lines
       l         D
       0.0111180 3.1350E-03
       0.0113720 9.6120E-03
       0.0116200 4.3270E-02
       0.0121960 2.7310E-10
       0.0123390 3.1290E-09
       0.0128090 1.4170E-01
       0.0129680 1.6020E+00
       0.0131270 3.7160E-01
       0.0132910 4.1460E+00
       0.0134420 1.4520E+00
       0.0136180 1.6130E+01
       0.0136620 6.7380E-10
```

0.0142360 7.2240E-10

0.0145110 3.2020E-01

0.0147490 4.1500E-10

0.0148250 1.9400E-08

0.0149530 3.6930E-01

0.0149700 2.9000E-01

0.0152360 1.3550E-07

0.0153500 6.8500E-01

0.0153750 5.6910E-09

0.0154000 1.1150E+00

0.0154470 7.7860E-10

0.0156050 7.1750E+00

0.0156410 1.8170E-01

0.0157270 2.4140E+00

0.0160070 1.6250E+01

0.0161040 1.2140E+01

0.0162020 5.1650E+01

0.0162090 2.2320E+00

0.0164100 5.5260E+01

0.0164260 3.0110E-01

0.0165770 9.3550E-01

0.0166390 5.1010E+00

0.0167080 5.3240E+01

0.0169310 1.9530E+01

0.0170680 1.7680E+01

0.0172220 1.2700E+00

0.0174540 1.4330E-02

0.0178480 2.2070E-09

0.0184120 8.3830E-10

0.0189800 1.2010E+00

0.0193040 1.4200E-02

0.0195050 1.6710E-02

0.0195710 1.4810E+00

0.0195990 4.3530E-01

0.0198880 1.0930E+00

0.0201010 1.2350E+00

0.0201690 4.8060E+00

0.0202170 5.1100E-01

0.0204870 9.4950E-02

0.0207150 1.0500E-01

0.0208440 1.6080E+00

0.0434900 8.2100E-02

0.0450000 3.4380E-03

0.0454500 2.1500E-02

0.0465390 4.7570E-09

0.0532000 6.3000E-03

0.0532280 1.6100E-08

0.0549600 3.0250E-02

0.0554500 4.5020E-02

0.0582000 1.6850E-02

0.0591900 6.6420E-02

0.0627000 3.8470E+00

0.0632400 5.7520E+03

0.0672500 1.1080E-01

0.0676720 3.7860E-06

0.0694600 5.9160E-02

0.0741380 3.0270E-10

0.0748150 1.8400E-07

0.0761720 1.6530E-10

0.0768630 2.4070E-08

0.0771070 3.3370E-07

0.0792900 4.4180E-08

0.0798400 3.0930E-01

0.0810690 9.2210E-09

0.0837870 1.6760E-08

0.0846830 2.1320E-10

0.0854310 8.3640E-08

0.0868300 5.7700E-08

0.0873490 1.0550E-07

0.0878920 3.2790E-09

0.0884710 1.5060E-07

0.0891780 2.1100E-01

0.0892560 7.2060E-09

0.0897840 4.2270E-08

0.0898070 1.4020E-08

0.0899570 7.3410E+01

0.0900740 1.0820E-08

0.0903630 4.4290E-10

0.0914910 6.7740E+00

0.0922820 2.3100E+03

0.0923170 5.5700E-09

0.0923500 1.3020E+04

0.0926180 1.5760E-09

0.0927800 7.9430E+03

0.0933500 1.4290E+02

0.0938440 5.3580E+01

0.0942470 2.7320E-09

0.0946540 1.5800E+04

0.0948680 5.3100E-09

0.0954490 1.7690E-10

0.0958630 4.0850E+03

0.0971700 2.0050E+00

0.0975300 2.1380E-09

0.0978530 6.9780E-10

0.0984340 2.8650E+04

0.0994320 2.4800E-08

0.0998600 2.9000E+01

0.1001300 4.7860E-08

0.1007390 1.6700E-09

0.1008900 1.1530E+00

0.1029480 1.9550E-08

0.1032960 6.7750E-09

0.1034000 8.1030E-03

0.1037700 2.3750E+00

0.1048190 1.9290E+01

0.1056040 3.9320E+01

0.1062390 1.4640E+00

0.1066800 3.8780E-01

0.1072200 1.5000E-09

0.1075950 6.8710E+02

0.1084220 1.2610E+03

0.1085830 1.6880E+01

0.1089550 5.6740E+00

0.1090720 4.9780E+01

0.1100000 2.2230E-09

0.1104210 4.8990E+03

0.1112980 9.5110E+03

0.1114860 5.2600E+02

0.1118700 1.8190E+02

0.1119640 3.5790E+02

0.1128000 2.1450E+03

0.1144450 3.9790E+03

0.1148440 1.4360E+03

0.1209000 4.1830E-03

0.1254600 3.0080E+00

0.1313000 7.8010E+01

0.1346100 5.2310E-01

0.1372300 1.3000E-01

0.1374500 2.6840E-10

0.1401500 2.5860E+00

0.1409100 1.6060E+00

0.1413000 1.9210E-10

0.1437800 1.7480E+00

0.1438720 8.5840E-07

0.1498800 4.3880E-01

0.1527100 3.8130E+01

0.1594800 4.6230E+00

0.1596000 3.4360E-04

0.1649400 3.9940E-01

0.1656100 5.6490E-01

0.1700700 2.4600E-09

0.1708500 4.2750E+00

0.1745500 1.4730E+00

0.1798000 4.2600E-01

0.1860530 2.9520E-07

0.1861500 1.8460E+01

0.1862110 3.4650E-07

0.1937300 5.7160E+00

0.1962000 7.5520E-09

0.1968000 8.6620E-01

0.1999500 9.0040E-01

0.2009700 1.1330E+01

0.2031200 3.7760E+01

0.2051000 2.1960E-10

0.2056800 1.4120E-09

0.2164700 3.0540E-09

0.2200000 2.2670E+00

0.2210000 4.3770E-10

0.2211500 8.1990E-01

0.2218300 1.1560E+00

0.2265000 7.1160E+01

0.2269500 1.7670E+02

0.2272500 9.7960E+01

0.2300000 1.2830E-09

0.2322100 3.1290E+00

0.2350000 4.9460E-10

0.2351100 2.0850E+00

0.2384000 2.6170E-09

0.2402000 9.9640E-01

0.2419970 1.3420E-06

0.2453700 1.5290E+01

0.2477900 7.7110E-03

0.2492200 5.2100E+01

0.2528000 5.9980E-10

0.2537290 7.8320E-07

0.2538000 5.9850E-08

0.2572000 1.1670E+00

0.2582600 1.0420E+03

0.2588700 1.1060E-07

0.2622700 1.0900E-09

0.2671200 4.3240E+00

0.2688000 4.5980E-09

0.2722800 2.7880E+01

0.2738000 3.5950E-08

0.2748000 1.1450E-07

0.2750400 2.4450E+00

0.2783000 1.1150E+00

0.2809500 1.5230E-08

0.2937900 9.1130E+01

0.2952240 5.4620E-06

0.2959100 4.4690E+00

0.2960000 4.7330E-09

0.2987000 4.2350E-01

0.2987600 5.8080E-09

0.3042000 2.5370E-08

0.3052600 9.4310E-09

0.3086000 6.9890E-01

0.3102000 2.4730E+00

0.3105200 4.6040E-03

0.3135000 3.6140E+00

0.3143200 2.5260E-08

0.3167000 3.6930E+00

0.3204000 1.8920E+00

0.3238300 9.6550E-09

0.3304000 3.0260E+01

0.3314000 2.8420E+00

0.3333100 2.9300E-08

0.3347800 2.5130E-08

0.3402000 1.6710E+00

0.3438000 1.4450E+00

0.3489200 4.8250E-08

0.3519000 1.8360E+01

0.3519320 1.5380E-05

0.3560000 3.2790E-09

0.3579000 1.6620E+00

0.3606000 8.1930E-01

0.3634700 3.4030E-09

0.3650000 8.3920E-01

0.3695000 1.2140E+02

0.3720000 6.0470E+01

0.3755900 2.1410E-09

0.3791000 2.1260E+00

0.3820000 2.9980E-10

0.3854000 2.1950E+00

0.3867700 1.5260E-07

0.3879400 3.8340E-02

0.3888800 1.8410E-07

0.3940500 7.5510E-09

0.3941000 5.1530E+00

0.3960100 1.4930E-08

0.3977000 1.5140E+00

0.4018000 2.0780E+00

0.4057400 9.1620E-08

0.4098000 2.0330E+01

0.4146000 1.6870E-10

0.4161000 2.2170E+00

0.4253000 2.3070E+00

0.4269500 2.9210E+01

0.4274000 1.9950E-03

0.4280000 1.3670E-09

0.4331000 6.1300E+00

0.4393400 7.4730E-09

0.4466000 7.9110E+00

0.4493700 1.2340E-10

0.4509300 2.7790E-01

0.4509600 1.3290E+02

0.4524000 1.9120E+00

0.4529200 2.0360E-08

0.4535800 8.5050E+01

0.4547700 1.9850E-07

0.4549500 6.3280E-05

0.4586800 8.2860E+01

0.4610000 3.5890E-08

0.4615000 2.5120E+00

0.4620000 1.5020E-07

0.4642000 2.3070E+00

0.4680000 1.6370E+01

0.4684400 1.0880E+02

0.4697600 9.0210E-08

0.4723000 2.7710E+01

0.4742000 2.7900E+00

0.4744100 7.8220E-08

0.4757500 1.1170E+02

0.4786000 9.7160E+00

0.4800000 3.0140E-10

0.4804300 2.3240E-07

0.4810000 2.4490E+01

0.4859200 1.6280E-08

0.4867000 4.4520E-09

0.4870900 3.1350E-07

0.4879500 2.0870E-08

0.4942000 9.1320E-09

0.4969000 5.2980E-09

0.4980000 5.1870E+00

0.5019600 1.4050E-08

0.5020000 2.2770E+00

0.5035000 2.8490E-06

0.5067500 1.1120E+02

0.5082000 4.5670E-05

0.5100000 6.0860E-08

0.5110000 2.5700E-08

0.5134000 6.6290E+01

0.5196000 3.5170E+01

0.5199000 1.3210E-08

0.5214000 6.7000E+01

0.5246000 1.4240E-08

0.5279000 3.6060E+01

0.5280000 3.3840E-09

0.5291000 8.5710E+00

0.5336600 1.6000E-07

0.5341000 7.7310E+00

0.5367700 5.9020E-08

0.5372000 7.8010E+00

0.5384100 1.7440E-08

0.5430000 7.4220E-08

0.5438000 1.2920E+01

0.5438100 6.1090E-08

0.5439800 2.1680E+02

0.5476000 3.5800E-09

0.5518000 1.7270E-10

0.5537000 4.3920E+00

0.5580000 9.3000E+00

0.5592000 7.2570E+00

0.5628000 3.6640E+00

0.5652000 1.0530E+02

0.5689000 3.7230E+02

0.5695000 8.5240E+02

0.5705000 1.1100E-09

0.5727600 7.0870E-08

0.5755000 2.8140E+00

0.5801300 3.4350E-07

0.5817000 4.4960E-05

0.5841000 1.8800E+01

0.5863000 7.7850E+00

0.5903000 3.9310E+00

0.5952300 1.7220E-08

0.5954000 1.0240E+01

0.5969000 2.1690E+01

0.6000000 8.1990E-09

0.6006600 5.0410E-10

0.6026000 6.0170E+01

0.6046000 5.8130E+00

0.6093120 4.8300E-05

0.6120000 4.3760E+01

0.6157300 6.3800E-08

0.6170000 5.9820E+00

0.6190000 4.2070E+00

0.6200000 2.9950E-10

0.6242000 4.1350E+01

0.6244000 3.4000E-06

0.6264000 5.4460E-09

0.6281000 2.8210E+01

0.6294000 4.1830E+01

0.6307900 3.9590E-08

0.6326000 4.3360E+00

0.6331400 6.0800E-08

0.6343000 1.6160E+01

0.6347200 7.2100E-09

0.6396700 3.3630E-08

0.6432000 3.2950E+00

0.6465000 1.4040E+01

0.6491800 6.8640E-08

0.6515000 2.2990E-09

0.6537000 5.8300E+01

0.6543700 1.7320E+02

0.6552000 1.6900E+01

0.6574000 4.9610E+01

0.6587000 1.7500E-08

0.6598000 3.4110E+01

0.6611000 5.5100E-08

0.6639000 6.8790E+01

0.6654530 1.7270E-06

0.6665000 1.5030E+02

0.6697000 1.2850E+02

0.6700000 4.9600E-10

0.6751000 1.3120E+01

0.6774100 7.2650E-09

0.6776000 4.6320E-06

0.6832200 9.9190E-08

0.6839000 2.0640E+01

0.6851000 1.9300E+01

0.6876000 8.5200E-09

0.6910800 6.6010E+02

0.6926000 1.6780E+02

0.6933000 7.4890E-09

0.6979000 6.4200E-08

0.6990300 4.9540E+02

0.6998200 2.0210E-08

0.7020500 6.1220E+02

0.7031100 5.9990E-07

0.7049000 5.9930E-08

0.7059000 8.7970E+02

0.7083000 3.1670E+00

0.7088000 2.1830E-08

0.7106700 9.6630E-08

0.7115000 2.1720E+01

0.7137000 2.0350E+01

0.7165000 4.3820E+00

0.7198600 4.9630E-07

0.7229800 4.6080E-08

0.7278000 1.6390E+01

0.7309000 9.1350E+01

0.7333900 1.0080E+03

0.7338000 5.7670E-08

0.7380000 1.6970E+02

0.7399500 1.0870E+03

0.7407300 5.4280E-08

0.7427700 7.4160E+03

0.7428100 3.0560E+02

0.7459000 4.7600E+01

0.7481000 1.5410E+01

0.7528400 1.7990E-07

0.7550000 1.8390E+02

0.7589000 3.7640E+01

0.7610000 1.1010E+01

0.7648000 3.0080E+01

0.7659600 1.1020E-07

0.7663700 2.8310E+04

0.7664000 1.1110E+01

0.7683560 7.0090E-06

0.7691000 2.8690E+01

0.7697000 4.2650E-08

0.7724000 1.1210E+01

0.7786000 7.1160E+00

0.7804000 1.4110E+02

0.7817300 7.6910E+02

0.7834000 4.7250E+01

0.7859600 1.5590E-06

0.7861000 4.5190E-07

0.7862500 4.8150E+03

0.7862700 1.8980E+02

0.7886000 2.1950E-08

0.7928000 7.1050E+00

0.7949000 1.0770E+02

0.7961000 4.1510E+02

0.7964200 5.4430E+02

0.7996000 3.0910E-08

0.7997000 1.5400E-08

0.8023000 5.0260E+00

0.8031000 2.2370E-10

0.8041000 1.0080E+02

0.8057400 8.9760E+02

0.8058000 4.1260E+02

0.8061740 1.8320E-06

0.8082000 2.6620E+02

0.8084000 5.9160E+00

0.8115000 2.0370E+01

0.8142000 5.1130E+01

0.8150000 5.7780E-08

0.8192000 3.1410E+02

0.8211800 2.4230E-07

0.8242000 2.0740E+02

0.8251000 3.1670E+02

0.8263000 1.6990E-07

0.8293000 6.0910E+01

0.8315000 6.9830E+02

0.8323900 4.3620E-08

0.8390400 9.2250E-07

0.8395000 5.2940E+00

0.8404000 1.4170E-08

0.8441000 7.2800E+01

0.8461000 8.9010E+00

0.8471600 4.1310E-08

0.8489000 4.6460E+00

0.8515700 7.6040E+02

0.8518000 1.2560E+01

0.8577000 6.3260E+00

0.8600000 2.3500E-09

0.8632000 1.2740E+01

0.8697000 3.4870E+01

0.8730700 2.9570E-08

0.8740000 6.4590E+00

0.8760000 4.5330E+02

0.8780300 1.9840E-08

0.8805000 2.8190E+03

0.8832400 2.6040E+03

0.8872800 8.0690E+02

0.8901000 4.8940E+00

0.8986700 5.9910E+02

0.9042000 6.3180E+01

0.9042900 1.4510E-07

0.9100000 1.0710E-09

0.9157400 4.4970E-08

0.9165000 4.4670E+00

0.9178000 8.6690E-09

0.9184000 1.8690E+01

0.9205000 5.4640E+00

0.9217000 1.5030E+03

0.9250000 1.4910E+03

0.9266100 2.2860E+03

0.9302000 5.8030E-08

0.9340610 5.3510E-06

0.9341000 8.8310E-08

0.9345000 1.7670E-08

0.9358000 1.2710E+01

0.9386500 2.3080E-08

0.9396000 3.1990E-08

0.9419400 3.0280E+02

0.9420000 8.7960E+00

0.9433400 3.0330E-08

0.9459000 4.0750E+03

0.9474300 3.7830E+02

0.9477000 3.1580E+02

0.9498000 9.8840E-09

0.9522000 1.0810E-08

0.9527000 1.6180E+01

0.9600000 1.4270E+01

0.9616100 2.1840E-08

0.9640800 6.6060E-07

0.9650000 1.8270E-08

0.9658000 9.4360E+01

0.9751000 5.3860E+00

0.9761800 3.5120E-08

0.9782000 1.8080E+01

0.9803000 6.0660E+02

0.9816000 1.4600E+02

0.9842000 3.2830E+02

0.9893400 1.8730E-08

0.9895000 2.1020E+01

0.9914900 1.8780E-08

0.9920000 1.6860E+01

0.9946000 1.2680E+01

0.9949300 7.3120E+02

0.9977000 9.3270E+00

1.0009900 1.0800E+05

1.0099000 1.3730E+01

1.0138000 1.5930E-08

1.0195000 5.6310E+00

1.0210000 2.7060E-08

1.0218000 3.0390E+01

1.0236000 1.3050E+01

1.0253000 1.0890E+01

1.0287000 1.2020E+02

1.0323700 1.5240E-07

1.0328000 3.7290E+00

1.0333000 4.6940E-08

1.0359000 5.5000E+00

1.0379000 3.7470E+00

1.0380000 1.6310E-08

1.0411000 6.8540E+00

1.0417000 1.6080E+02

1.0444000 6.6530E+00

1.0456000 5.1440E-08

1.0514000 1.3390E+01

1.0519600 6.2690E-07

1.0578000 3.8160E+00

1.0618600 3.1400E+02

1.0651000 5.8750E+00

1.0672000 5.4480E-08

1.0699600 5.5620E-07

1.0700000 5.0440E-09

1.0736000 2.2770E+01

1.0832000 1.1250E+02

1.0842500 1.6730E+02

1.0853000 5.9800E+00

1.1036400 2.0820E-07

1.1047900 1.6050E-07

1.1069000 1.8740E+01

1.1100000 3.0450E-09

1.1106000 1.4100E+01

1.1189000 8.4320E-08

1.1202870 3.1870E-05

1.1217000 5.6900E+01

1.1249300 6.0570E+02

1.1252000 8.3210E+01

1.1268000 6.9030E+01

1.1302900 8.5100E-08

1.1336600 5.2900E-07

1.1514000 7.5220E+00

1.1535000 1.0690E+01

1.1551900 3.5350E-06

1.1556000 3.4710E-08

1.1560000 1.5190E-08

1.1673000 2.6260E-08

1.1713000 2.1430E+01

1.1729800 1.1210E-07

1.1731000 1.0850E+01

1.1821000 2.2340E+00

1.1936900 2.0460E+03

1.1940000 5.0070E+00

1.2076800 1.0160E-06

1.2100000 7.9700E-09

1.2173000 5.3420E+01

1.2203700 1.3900E+02

1.2204000 1.5290E+01

1.2267000 8.2130E-08

1.2306000 3.4310E-08

1.2372400 8.2760E+02

1.2373000 2.3200E+00

1.2381100 1.3310E-05

1.2412000 5.6850E+01

1.2478000 5.4500E+00

1.2526000 4.4250E+00

1.2565000 1.4870E+01

1.2777000 1.1370E+01

1.2790000 2.8300E-08

1.2809600 3.3760E-06

1.2840000 2.6020E-08

1.2851000 4.0230E-08

1.2928000 1.2000E+02

1.2964000 7.4840E+00

1.3012000 4.5570E+00

1.3037600 2.6790E-07

1.3160000 1.0510E-08

1.3169600 1.9280E-07

1.3270000 4.6230E+00

1.3300000 2.6700E-08

1.3414900 5.3740E-08

1.3429000 3.2910E+00

1.3529000 3.0880E+02

1.3546000 3.5870E+01

1.3590000 4.1480E+01

1.3776690 9.9520E-06

1.3853100 1.8900E-06

1.3896000 1.9650E+01

1.3925000 4.7610E-08

1.3935700 5.6260E+02

1.3975000 2.2550E+01

1.4003000 4.7980E+01

1.4015000 3.1960E-06

1.4079800 5.4270E-06

1.4091000 1.2180E+01

1.4100000 2.6250E-09

1.4138800 3.9570E+02

1.4144000 7.3850E-01

1.4197000 1.2940E-08

1.4269000 4.5700E+01

1.4341300 1.6840E+03

1.4428000 8.6280E+00

1.4454000 8.9260E+01

1.4527000 2.2530E+02

1.4589000 2.6060E+01

1.4709000 2.3860E-08

1.4758000 2.3320E+00

1.4791500 1.3270E-07

1.4854000 8.4860E+00

1.4880000 3.8080E+00

1.4900000 1.0860E-09

1.4936000 2.9350E+01

1.4960000 1.0280E+01

1.5000000 3.2370E+00

1.5073000 5.6050E+00

1.5092280 5.5520E-06

1.5101000 2.6580E+00

1.5102000 2.3080E+03

1.5155000 1.8200E-08

1.5156000 2.0710E+01

1.5207000 2.6680E+00

1.5272700 4.3200E+02

1.5385000 9.9960E-07

1.5388000 3.8780E+00

1.5400000 1.1060E-09

1.5433200 5.3260E-07

1.5481200 2.5420E+02

1.5501000 2.0960E+01

1.5537400 1.4710E+03

1.5670000 3.3130E+00

1.5706700 2.0090E+02

1.5799000 2.1170E+01

1.5832200 1.8620E-06

1.5859000 4.2420E+01

1.5900000 1.1240E-09

1.5916500 3.5000E+02

1.5938800 4.9690E+02

1.5940000 9.1130E+01

1.5947300 6.7700E-07

1.5950000 1.3540E-08

1.5980000 1.6260E-08

1.5993100 6.2370E-07

1.6018000 8.6710E+01

1.6183000 2.7540E+00

1.6273000 2.2400E+01

1.6363000 3.2910E-08

1.6370000 1.6460E-08

1.6381000 6.1570E+01

1.6405000 3.0810E+00

1.6449000 3.0850E+00

1.6500000 1.1440E-09

1.6502000 1.5450E+00

1.6546000 4.6920E+01

1.6557000 7.7350E+00

1.6570000 1.2690E-07

1.6612800 3.1760E-06

1.6648000 5.2730E+00

1.6658000 2.2950E-08

1.6684000 2.2980E+02

1.6728000 1.0260E+01

1.6795000 2.3050E+01

1.6839900 6.0030E-07

1.6857000 9.3590E+01

1.6861000 6.6260E+01

1.6938000 2.0950E+02

1.6943000 8.5380E+01

1.6950000 8.1320E+01

1.7005000 3.1320E+01

1.7110000 5.0380E-09

1.7197000 5.3510E+00

1.7232000 4.7260E+00

1.7278000 5.9930E+00

1.7295950 8.2120E-06

1.7377000 2.2770E+01

1.7377300 4.0610E+03

1.7411000 1.4870E+01

1.7432000 1.0130E+01

1.7500000 1.9660E+01

1.7514000 2.5450E-09

1.7575000 7.3080E+00

1.7598100 2.6960E+02

1.7644940 4.3680E-05

1.7654400 1.6780E+03

1.7680000 6.0520E+00

1.7708000 2.0720E+01

1.7730000 2.0730E+01

1.7837000 7.6730E+00

1.7968000 9.7280E+01

1.7971000 7.3750E+01

1.8058000 1.6060E+00

1.8090400 7.2070E+02

1.8137300 3.1550E-08

1.8153000 2.8980E+00

1.8192000 4.0210E-09

1.8196900 1.7570E+02

1.8198000 1.2890E+00

1.8251000 2.9040E+00

1.8308000 1.2920E+00

1.8313600 3.3720E+03

1.8380000 1.2940E+01

1.8383600 1.0380E-06

1.8474200 6.0960E-06

1.8498000 8.7570E+00

1.8630900 2.3640E+02

1.8676800 1.8140E+03

1.8728000 1.1080E+01

1.8731600 6.3610E-07

1.8748500 1.6190E+03

1.8772100 3.2650E+02

1.8841000 4.8990E+00

1.8901000 4.5780E+01

1.8903000 2.3310E-07

1.8934000 1.9630E+00

1.8935000 4.3610E+02

1.8959200 4.6680E-07

1.8967000 3.2740E+01

1.8987000 1.6640E-07

1.9111700 1.2530E+03

1.9155000 6.2430E+00

1.9254000 9.5460E+01

1.9279000 1.7120E+01

1.9284000 1.3990E+01

1.9352000 2.9680E+00

1.9355000 1.2050E-07

1.9370100 5.7950E+02

1.9377000 1.3200E+01

1.9572000 7.0310E+00

1.9580000 3.1790E+00

1.9692000 8.0520E+01

1.9712000 8.6280E-01

1.9774000 5.3150E+00

1.9779000 7.0560E+00

1.9896000 2.3300E+00

1.9946000 1.4850E-08

2.0010000 1.4170E+01

2.0100000 4.3300E-09

2.0107800 1.3990E-07

2.0216000 5.9650E-08

2.0223000 2.6400E+01

2.0414000 1.8330E+01

2.0529400 2.0680E-07

2.0660000 1.4310E+01

2.0722000 1.3490E+00

2.0851000 2.7400E-08

2.0897000 1.5070E-07

2.0900000 3.1310E-09

2.1019000 8.2200E+00

2.1099200 2.6590E-07

2.1185500 3.4490E-06

2.1200000 2.1180E-08

2.1366000 1.0320E+01

2.1479000 4.2520E-08

2.1604000 5.4750E-09

2.1765000 9.7540E-09

2.1925800 1.0380E-07

2.2042100 1.5540E-05

2.2516000 1.6910E-08

2.2603000 2.6780E-08

2.2665100 5.5440E-08

2.2700000 1.9210E-09

2.2709000 4.0060E-09

2.2843000 1.5740E-08

2.2876500 1.4200E-08

2.2934000 9.4200E-07

2.3102000 4.3320E-09

2.3124000 2.7850E-08

2.3193000 1.2390E-09

2.3250000 5.2670E-09

2.3313000 6.8520E-08

2.3480000 4.3470E-10

2.3535000 1.2430E-09

2.3600000 5.1690E-09

2.3610000 5.2860E-09

2.3690000 8.4010E-09

2.3769000 2.7400E-08

2.3908000 4.9880E-09

2.4051000 1.2800E-09

2.4232700 1.4380E-08

2.4300000 5.8500E-09

2.4447000 2.5050E-08

2.4478600 4.9180E-06

2.4828000 4.7110E-09

2.5054000 1.7930E-08

2.5507000 1.4520E-09

2.5530000 3.1570E-10

2.5620000 5.6850E-10

2.5640000 4.4230E-10

2.6045000 1.2670E-09

2.6309000 2.5380E-09

2.6624000 9.5330E-10

2.6947000 9.8680E-08

2.6994000 8.9150E-09

2.7193000 5.7370E-09

2.7699000 7.9870E-08

2.7859000 1.7580E-08

2.8270000 7.3660E-09

2.8611000 1.2190E-09

2.8803000 2.9520E-08

2.8935000 1.9260E-08

2.9219000 4.4990E-08

2.9286000 3.5360E-09

2.9346000 1.4790E-09

2.9789000 4.4430E-08

3.0000000 2.8350E-08

3.0539000 6.7740E-08

3.0817000 1.5490E-08

3.0940000 1.4210E-09

3.1426000 3.8780E-09

3.1490000 2.8440E-10

```
      3.1606000 1.0340E-09
      3.1836000 4.1720E-09
      3.2332000 3.2360E-10
      3.2697000 1.9430E-10
#     si3       sp3 $             The photon groups
      h         D
      0.0200000 0.0000E+00
      0.0397620 7.4306E+03
      0.0524070 7.4659E+03
      0.0669240 1.7014E+04
      0.0833300 2.4300E+04
      0.1016360 9.3583E+04
      0.1218530 1.5709E+03
      0.1439900 8.1044E+03
      0.1680530 1.0016E+04
      0.1940500 1.2090E+04
```

0.2219850 1.4605E+04

0.2518640 1.7371E+04

0.2836890 2.0151E+04

0.3174660 2.2683E+04

0.3531970 2.5054E+04

0.3908850 2.7040E+04

0.4300000 2.8177E+04

0.4700000 2.8413E+04

0.5100000 2.7705E+04

0.5120000 2.8670E+03

0.5612580 3.2561E+04

0.6087670 2.9575E+04

0.6582460 2.8669E+04

0.7096970 2.7467E+04

0.7631200 2.5854E+04

0.8185180 2.4296E+04

0.8758910 2.0778E+04

0.9352410 1.8881E+04

0.9965690 1.6936E+04

1.0598800 1.5392E+04

1.1251600 8.4511E+03

1.1924300 6.9600E+03

1.2616800 5.6238E+03

1.3329100 4.4210E+03

1.4061200 3.4678E+03

1.4813200 2.6691E+03

1.5585000 1.9362E+03

1.6376700 1.4083E+03

1.7188300 1.0453E+03

1.8019700 7.5939E+02

1.8870900 3.8903E+02

1.9742100 1.2834E+02

2.0633100 2.9399E+01

2.1544000 8.9710E+00

2.2474800 2.3170E+00

2.3425500 1.3720E+00

2.4396100 1.2680E+00

2.5386600 1.1870E+00

2.6397000 1.1050E+00

2.7427400 1.0210E+00

2.8477600 9.3810E-01

2.9547800 8.5900E-01

3.0637800 7.8100E-01

3.1747800 7.1400E-01

3.2877800 6.6020E-01

3.4027600 6.0640E-01

3.5197400 5.5080E-01

3.6387200 4.9930E-01

3.7596900 4.6170E-01

3.8826500 4.2640E-01

4.0076000 3.9010E-01

4.1345600 3.5220E-01

4.2635000 3.1330E-01

4.3944400 2.7640E-01

4.5273800 2.4700E-01

4.6623100 2.1890E-01

4.7992400 1.9170E-01

4.9381700 1.7030E-01

5.0790900 1.5150E-01

5.2220100 1.3440E-01

5.3669200 1.1900E-01

5.5138400 1.0650E-01

5.6627500 9.4330E-02

5.8136500 8.2220E-02

5.9665600 7.2170E-02

6.1214600 6.4470E-02

6.2783600 5.6970E-02

6.4372600 4.9280E-02

6.5981500 4.1400E-02

6.7610500 3.3440E-02

6.9259400 2.6280E-02

7.0928300 2.1560E-02

7.2617200 1.7430E-02

7.4326100 1.3440E-02

7.6055000 1.0300E-02

7.7803900 7.8820E-03

7.9572800 5.9200E-03

8.1361600 4.1640E-03

8.3170500 2.9370E-03

8.4999300 2.1220E-03

8.6848200 1.3500E-03

8.8717000 5.9590E-04

9.0605900 1.0060E-04

9.2514800 1.3720E-05

9.4443600 1.8610E-06